Copy No. _____

Guide for Mechanistic-Empirical Design
OF NEW AND REHABILITATED PAVEMENT STRUCTURES

FINAL DOCUMENT

APPENDIX KK:
TRANSVERSE CRACKING OF JPCP

NCHRP

Prepared for
National Cooperative Highway Research Program
Transportation Research Board
National Research Council

Submitted by
ARA, Inc., ERES Division
505 West University Avenue
Champaign, Illinois 61820

August 2003

Acknowledgment of Sponsorship

This work was sponsored by the American Association of State Highway and Transportation Officials (AASHTO) in cooperation with the Federal Highway Administration and was conducted in the National Cooperative Highway Research Program which is administered by the Transportation Research Board of the National Research Council.

Disclaimer

This is the final draft as submitted by the research agency. The opinions and conclusions expressed or implied in this report are those of the research agency. They are not necessarily those of the Transportation Research Board, the National Research Council, the Federal Highway Administration, AASHTO, or the individual States participating in the National Cooperative Highway Research program.

Acknowledgements

The research team for NCHRP Project 1-37A: Development of the 2002 Guide for the Design of New and Rehabilitated Pavement Structures consisted of Applied Research Associates, Inc., ERES Consultants Division (ARA-ERES) as the prime contractor with Arizona State University (ASU) as the primary subcontractor. Fugro-BRE, Inc., the University of Maryland, and Advanced Asphalt Technologies, LLC served as subcontractors to either ARA-ERES or ASU along with several independent consultants.

Research into the subject area covered in this Appendix was conducted at ARA-ERES. The authors of this appendix are Mr. Tom Yu and Dr. Michael Darter. Dr. Khazanovich provided the neural networks to compute stresses at the critical locations in JPCP. Data used in model calibration and verification was assembled by Mr. Leslie Titus-Glover.

Foreword

This appendix describes the mechanistic-empirical concepts involved and the development and calibration of the transverse crack prediction model for jointed plain concrete pavements (JPCP). These pavements are commonly constructed on new alignments, or for reconstruction projects, or as overlays of existing pavements. Transverse cracking initiates at either longitudinal edge of a slab (at the top or bottom of the slab) and progresses either transversely or diagonally across the slab until it reaches either the other longitudinal joint or a transverse joint (this would essentially be a diagonal crack). The key point is that it initiates at one or the other longitudinal joint. This type of cracking is considered the primary structural fatigue distress type of JPCP. All levels of transverse crack severity are included in the calibration data base.

The information contained in this appendix serves as a supporting reference to discussions presented in PART 3, Chapters 4 and 7 of the Design Guide.

APPENDIX KK
TRANSVERSE CRACKING OF JPCP

1.0 INTRODUCTION

This appendix describes the mechanistic-empirical concepts involved and the development and calibration of the transverse crack prediction model for jointed plain concrete pavements (JPCP). These pavements are commonly constructed on new alignments, or for reconstruction projects, or as overlays of existing pavements. Transverse cracking initiates at either longitudinal edge of a slab (at the top or bottom of the slab) and progresses either transversely or diagonally across the slab until it reaches either the other longitudinal joint or a transverse joint (this would essentially be a diagonal crack). The key point is that it initiates at one or the other longitudinal joint. This type of cracking is considered the primary structural fatigue distress type of JPCP. All levels of transverse crack severity are included in the calibration data base.

This procedure does not include the prediction of longitudinal cracking which initiates at a transverse joint at either the top or bottom of the slab, and progresses along the slab to the next transverse joint, but may also propagate to a longitudinal joint. Longitudinal cracking is often caused by inadequate longitudinal joint forming procedures and wanders around the longitudinal lane to lane joint. These cracks occur within the first few years of pavement life and are not the result of repeated load fatigue damage. Sometimes, however, longitudinal cracks appear to initiate either in the wheel paths or between the wheel paths and progress along the wheel paths. This often occurs when the slab is fairly thin (e.g., < 7 in as was well documented at the AASHO Road Test) this is believed to be a form of fatigue cracking in the wheelpaths. For thicker slabs it is a rare occurrence and is difficult to explain mechanistically as a fatigue based fracture since the damage calculated at various points is normally much less than damage for transverse cracking. However, longitudinal cracking does occur more often in widened slab JPCP designs and for that type of design may represent a form of fatigue initiated cracking. While this cracking model does not consider longitudinal cracking, future additions to this design procedure should fully consider this form of fracture.

This mechanistic-empirical prediction for fatigue cracking includes a comprehensive iterative damage accumulation algorithm. Damage is accumulated on a monthly basis considering both day time and nighttime hourly thermal gradients. The accumulated damage at the top and bottom of the slab is then correlated with field cracking of JPCP of projects located throughout North America. This correlation produces a calibrated model for slab transverse cracking of JPCP. Field data from hundreds of projects from LTPP and other sources are included in this calibration.

The calibration data is then used in the development of the design reliability procedure for JPCP cracking. This procedure is described in Appendix BB and is not reported herein in detail.

2.0 BASIC APPROACH AND CONCEPTS

Summary of Previous Mechanistic-Empirical Slab Cracking Models

There have been several previous studies to develop prediction models for transverse cracking of JPCP. These studies were both empirical and semi-empirical (statistical regression using limited structural responses) and mechanistic-empirical based (using structural responses to compute fatigue damage which is calibrated with field cracking). These key previous mechanistic-empirical based studies are briefly summarized below.

- The Portland Cement Association utilized beam fatigue data since the 1930's to directly consider fatigue fracture in design. The 1966 PCA design procedure (39) was a key development in that it utilized the full axle load spectra for single and tandem axles, a structural response model to calculate critical stresses at the transverse joint, and Minor's damage model (22) to compute fatigue damage to the slab. A revised version was published in 1984 (42) that more adequately utilized edge stress as the critical loading. The total fatigue damage value was limited to less than 100 percent (or a Minor's damage value of 1.00) to limit slab fracture. No attempt was made to correlate computed damage to actual field slab cracking other than general comparison with field performance. Factors considered in this procedure are as follows.
    - Axle load spectra distribution (single and tandem).
    - Three load positions (edge, joint and near edge).
    - Critical stress from loading with the axle at the transverse joint.
    - PCC strength was third-point beam 28-day strength.
    - Thermal curling or moisture warping were not considered.
    - Fatigue damage was computed considering only the 28-day strength.

- Darter and Barenberg (41) developed a fairly comprehensive fatigue damage procedure for JPCP in 1978 at the University of Illinois under contract to the FHWA. This procedure expanded the PCA procedure to include the following factors.
    - Axle load spectra distribution (single and tandem).
    - The edge loading position was identified as critical (loads were varied transversely across the slab using a normal distribution).
    - Critical stress was computed at the bottom of the slab using a 2D FEM based on axle loading, positive and negative thermal gradient, and an equivalent negative temperature gradient to represent moisture gradient of dry on top and wet on bottom).
    - PCC strength was third-point beam 28-day strength but it varied throughout the entire design life, month by month.
    - Both positive and negative thermal gradients were considered.
    - Moisture gradient through the slab was considered to be a negative 0.5 degree F per inch of slab.
    - Fatigue damage was computed both night and day throughout the entire design life (but only at the slab bottom edge longitudinal joint).
    - A good correlation was made between fatigue cracking from limited field projects and the computed accumulated fatigue damage (note that this was the first known

correlation between the theoretical damage calculated by Miner's damage model and field slab cracking).

- Poblete et al (38) developed a comprehensive fatigue damage procedure in the 1980's at the University of Chile that was similar to the University of Illinois approach to correlation of damage to field slab cracking. However, stresses at the top of the slab were identified as being the most critical in the dryer climate of Chile as cracks were found to initiate at the top of the slab. This procedure considered the following factors:
    - Axle load spectra distribution (single, tandem axles).
    - The wheel path loading position was used generally near the transverse joint for the non doweled joints.
    - Critical stress was computed at the top of the slab using a 3D FEM based on axle loading, negative thermal gradients, and an equivalent negative temperature gradient to represent the moisture gradient (dry on top and wet on bottom).
    - PCC strength was third-point beam 28-day strength.
    - Fatigue damage was computed for only nighttime temperature gradients only at the top of the slab.
    - A very good correlation was found between fatigue cracking from Chilean field projects and the computed accumulated fatigue damage at the top of the slab.

- A research team including Yu, Smith, Darter, Jiang and Khazanovich at ERES Consultants, Inc. under contract to the FHWA in the 1990's (2, 40). This procedure considered the following factors:
    - The edge loading position was identified as critical (however, loads were varied transversely across the slab following a normal distribution).
    - Critical stress was computed at the bottom of the slab using a 2D FEM based on axle loading, thermal gradients through the slab, and an equivalent negative temperature gradient to represent moisture gradient).
    - Axle load was limited to 18-kip ESAL.
    - PCC strength was third-point beam 28-day strength only.
    - Both positive and negative thermal gradients from solar radiation were considered.
    - Moisture gradient through the slab was approximately considered through an equivalent (negative) temperature gradient adjustment.
    - Fatigue damage was computed at the slab bottom edge both night and day throughout the entire design life (but only at the bottom of the slab but it was recognized that the top of the slab could be more critical under certain conditions such as dryer climates).
    - A good correlation was found between bottom up fatigue cracking from field projects (percent slabs cracked) and the computed accumulated fatigue damage and a calibrated cracking model developed (sections suspected of top down cracking were not included in the analysis).

- Several studies conducted on built-in temperature gradients at construction and moisture gradients through the concrete slab in the 1980's and 1990's lead to new knowledge on the initiation of slab cracking. These key studies were conducted in Chile (3, 38, 43, 44),

in Germany (9, 10, 11, 45, 50, 51), and the U.S. (4, 8, 37, 46, 47, 48, 49). They provided the technology that allowed the research team to include both a permanent built-in temperature gradient and permanent moisture gradient and a transitory temperature and moisture gradients in the design procedure in a practical manner.

The procedure developed under NCHRP 1-37A made full use of the knowledge and experience gained from these previous studies and others. The complete fatigue cracking algorithm developed as part of the design guide for JPCP considers truck axle loadings (four types of axles, lateral distribution, full axle load spectra), thermal gradients (non-linear, hourly, built-in), and moisture gradients (permanent shrinkage and transitory shrinkage) in more detail and extent than has been accomplished in the past to produce a comprehensive yet practical mechanistic-empirical cracking model (both bottom up initiated and top down initiated cracking are included). The remainder of this appendix describes in detail the mechanistic based algorithm developed to predict a combination of top down and bottom up transverse cracking of JPCP.

Critical Loadings and Stress Locations

Transverse cracking of PCC slabs can initiate either at the top surface of the PCC slab and propagate downward (top-down cracking) or vice versa (bottom-up cracking) depending on the loading and climatic conditions at the project site, as well as material properties and the conditions during construction. Both top-down and bottom-up cracking are considered in this Guide. Damage accumulates differently for each of these different distresses and hence needs to be computed separately. The following sections explain the damage accumulation process of these distresses.

Bottom-Up Transverse Cracking (JPCP)

When the truck axles are near the longitudinal edge of the slab, midway between the transverse joints, a critical tensile bending stress occurs at the bottom of the slab, as shown in figure 1. This stress increases greatly when there is a high positive temperature gradient through the slab (the top of the slab is warmer than the bottom of the slab). Repeated loadings of heavy axles under those conditions result in fatigue damage along the bottom edge of the slab, which eventually result in a transverse crack that is visible on the surface of the pavement and work their way across the slab. Over time, some transverse cracks in JPCP deteriorate and cause roughness. Major factors that affect bottom-up cracking are PCC thermal coefficient of expansion, slab thickness, joint spacing, slab widening, tied PCC shoulder, strength of PCC, and a stabilized base.

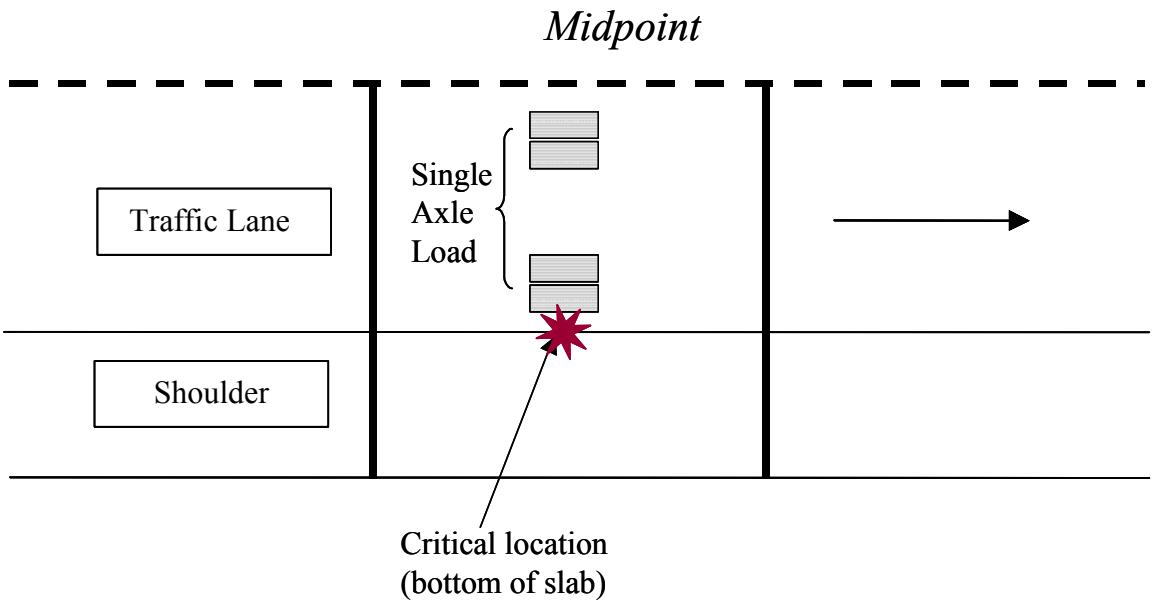

Figure 1. Critical load and structural response location for JPCP bottom-up transverse cracking.

Top-Down Transverse Cracking (JPCP)

Repeated loading by heavy trucks when the pavement is exposed to high negative temperature gradients (the top of the slab cooler than the bottom of the slab) or high shrinkage of the top of the slab compared to the bottom result in fatigue damage at the top of the slab, which eventually results in a transverse crack that is initiated on the surface of the pavement. The critical loading condition for top-down cracking involves a combination of axles that loads the opposite ends of a slab simultaneously. In the presence of a high negative temperature gradient, a moisture gradient, and such load combinations cause a high tensile stress at the top of slab near the middle of the critical longitudinal edge, as shown in figure 2 (*2, 3*). This type of loading is most often produced by the combination of steering and drive axles of truck tractors and other vehicles. Multiple trailers with relatively short trailer-to-trailer axle spacing are other common sources of critical loadings for top-down cracking. The top-down stress becomes critical when a significant amount of permanent upward curl/warp is present.

The same factors that affect bottom-up transverse cracking likely affect top-down cracking. In addition, the placement and curing of the concrete slab has a major effect. If the pavement is placed during conditions favorable to developing a high built-in temperature gradient (placed in the morning with high solar radiation) and no attempts to control this gradient through say water curing, the resulting high built-in gradient will significantly contribute to top down fatigue cracking.

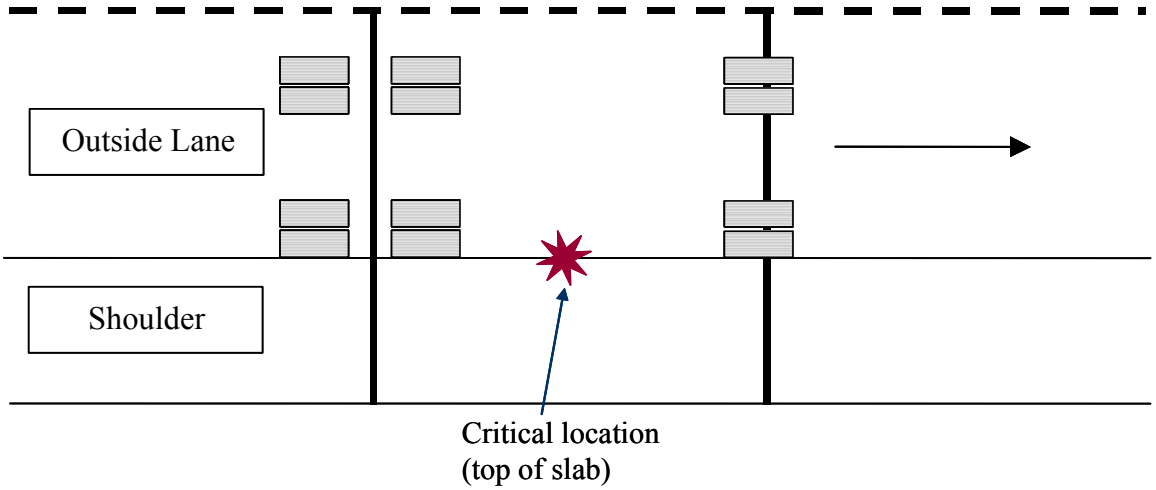

Figure 2. Critical load and structural response location for JPCP top-down transverse cracking.

3.0 KEY FACTORS IN SLAB CRACKING PREDICTION

Traffic Loadings

The Design Guide considers truck traffic loadings in terms of axle load spectra, as described in detail in PART 2, Chapter 4. The full axle load spectra for single, tandem, tridem, and quad axles are considered in the prediction of slab cracking. The ESAL approach is totally inadequate and is no longer used as a direct design input. A summary of the traffic data specifically related to predicting JPCP cracking is presented. Detailed discussion and guidance on traffic inputs is presented in PART 2, Chapter 4.

Basic Information

- Annual Average Daily Truck Traffic (AADTT) for base year – the total number of heavy vehicles (classes 4 to 13) in the traffic stream.
- Percent trucks in the design direction (directional distribution factor).
- Percent trucks in the design lane (lane distribution factor).
- Operational speed of vehicles – this input is used in the calculation of moduli of asphalt bound layers only.

PART 2, Chapter 4 discusses the recommended procedures to configure these inputs at each of the three hierarchical levels. Most of the sections used in JPCP calibration had traffic data at Level 1 and 2. Other sections utilized Level 3 data (national averages). Default values based on national traffic studies are presented in the chapter for use at Level 3 for the directional and lane distribution factors.

Traffic Volume Adjustment

Monthly Adjustment Factors

The truck monthly distribution factors are used to determine the monthly variation in truck traffic within the base year. These values are simply the ratio of the monthly truck traffic to the AADTT. Naturally, the average of the ratios for the 12 months of the base year must equal 1.0. PART 2, Chapter 4 discusses the monthly adjustment in more detail. Calibration utilized a uniform distribution (i.e., 1.0 for all months for all vehicle classes).

Vehicle Class Distribution

The normalized vehicle class distribution represents the percentage of each truck class (classes 4 through 13) within the AADTT for the base year. The sum of the percent AADTT of all truck classes should equal 100. PART 2, Chapter 4 discusses the procedures to determine this input at each of the input levels. It is important to note that if site-specific (Level 1) or regional data (Level 2) data were used for most JPCP sections. When not available, national truck traffic classification (TTC) data were used in conjunction with the functional class of the roadway to estimate the vehicle class distribution. Each TTC represents a traffic stream with unique truck traffic characteristics, and a default vehicle class distribution for each TTC using a national

traffic database for use at Level 3. The default values are provided in PART 2, Chapter 4 and Appendix AA. They are also a part of the Design Guide software.

Hourly Truck Traffic Distribution

The hourly distribution factors represent the percentage of the AADTT within each hour of the day. These factors are important in the prediction of JPCP cracking. They help accurately account for daytime and nighttime traffic streams required for cracking. PART 2, Chapter 4 was used in the calibration.

Traffic Growth Factors

The traffic growth function allows for the growth or decay in truck traffic over time (forecasting or backcasting truck traffic). The actual growth for JPCP calibration section was used.

Axle Load Distribution Factors

The axle load distribution factors simply represent the percentage of the total axle applications within each load interval for a specific axle type and vehicle class (classes 4 through 13). This input is very critical to prediction of slab cracking. This data needs to be provided for each month for each vehicle class. A definition of load intervals for each axle type is provided below:

Single axles – 3,000 lb to 41,000 lb at 1,000 lb intervals.
Tandem axles – 6,000 lb to 82,000 lb at 2,000 lb intervals.
Tridem and quad axles – 12,000 lb to 102,000 lb at 3,000 lb intervals.

The axle load spectrum measured at each site was used in the calibration. Where not available, the national average load distribution was used for the highway class of the JPCP section.

General Traffic Inputs

Most of the inputs under this category define the axle load configuration and loading details for calculating pavement responses. The exceptions are "Number of Axle Types per Truck Class" and "Wheelbase" inputs, which are used in the traffic volume calculations.

Mean Wheel Location

Distance from the outer edge of the wheel to the pavement marking. This input is very important in computing fatigue damage for both JPCP cracking. The sensitivity of JPCP transverse cracking to mean wheel location is shown in figure 3. As shown in this figure, mean wheel location is a very sensitive factor that affects JPCP cracking. Depending on the mean wheel location, the slab cracking can vary by a factor of 4 or more. If a typical-width (8.5-ft) truck were perfectly centered in a standard-width (12-ft) lane, the mean wheelpath would be 21 in. Site conditions and pavement design features such as tied PCC shoulder or widened slab may affect the mean wheelpath.

The estimation of this input at the three input levels is discussed in PART 2, Chapter 4. Calibration used 18 inches for this input since all sections had paved shoulders.

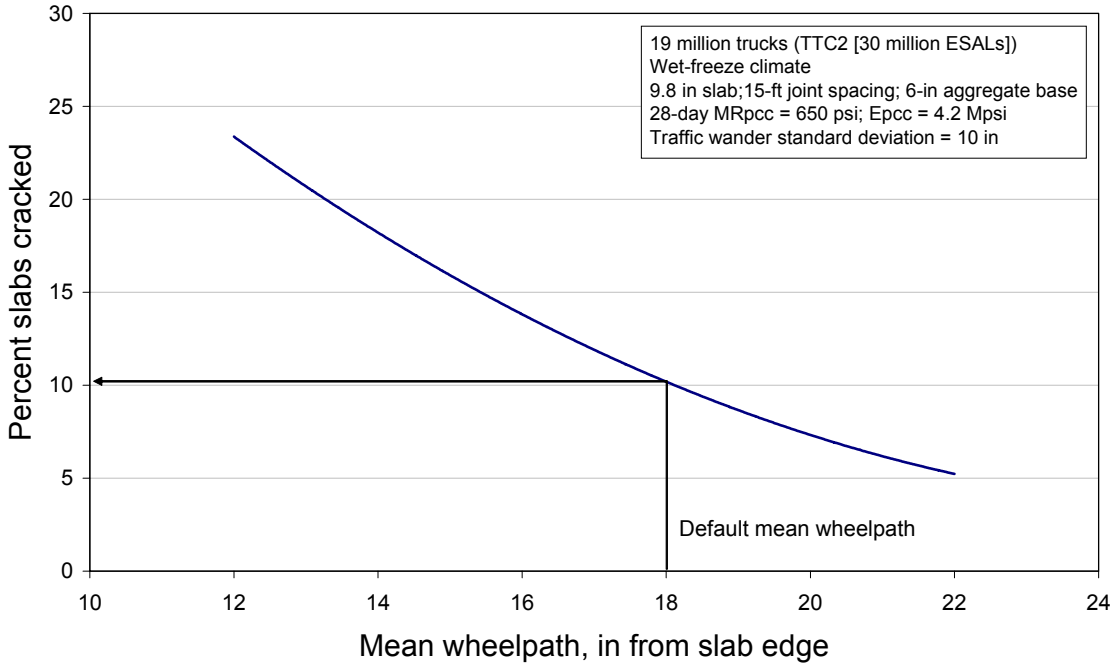

Figure 3. Sensitivity of JPCP transverse cracking to mean wheelpath.

Traffic Wander Standard Deviation

This is the standard deviation of the lateral traffic wander. The wander is used to determine the number of axle load applications over a point for predicting distress and performance. This parameter affects prediction of all pavement distresses, but it is a relatively insensitive factor, as shown in figure 4. Site conditions and pavement design features such as tied PCC shoulder or widened slab may affect the traffic wander standard deviation.

The estimation of this input at the three input levels is discussed in PART 2, Chapter 4. A value of 10 inches was used for this input based on previous studies. (2, 4, 41)

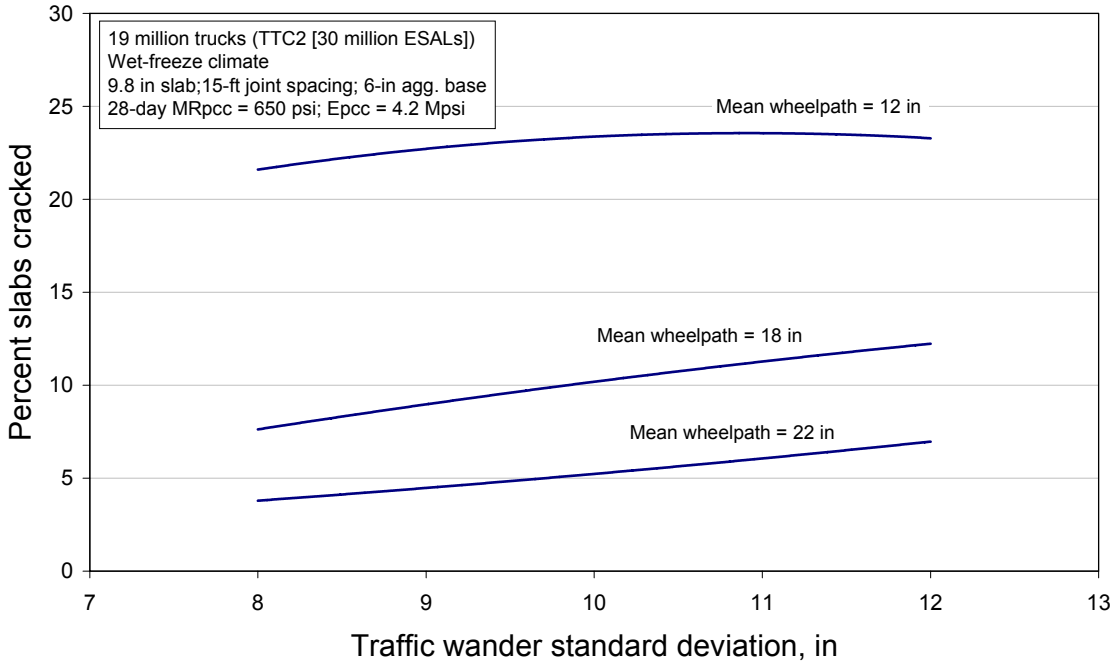

Figure 4. Sensitivity of JPCP transverse cracking to traffic wander standard deviation.

Axle Configuration

A series of data elements are needed to describe the details of the tire and axle loads for use in the pavement response module. Values used in calibration are provided below.

- Average Axle-Width – the distance between two outside edges of an axle. For typical trucks, 8.5 ft may be assumed for axle width.
- Dual Tire Spacing – the distance between centers of a dual tire. Dual tire spacing for trucks is 12 in.
- Tire Pressure – the hot inflation pressure or the contact pressure of a single tire or a dual tire. For heavy trucks, hot inflation pressure is 120 psi.
- Axle Spacing – the distance between the two consecutive axles of a tandem, tridem, or quad. The average axle spacing is 51.6 in for tandem and 49.2 in for tridem axles.

Wheelbase

This information is used in determining the number of load applications for JPCP top-down cracking. For top-down cracking, the critical loading is caused by a combination of axles that places an axle load close to both ends of a slab at the same time (figure 2). In general, the steering and drive axles of truck tractors or other trucks are the most common sources of these load combinations, but multiple trailers can also cause this type of loading. The inputs in this category include the following:

- Average axle spacing (ft) – short, medium, or long. The calibration values used are 12, 15, and 18 ft for short, medium, and long axle spacing, respectively.

- Percent of trucks – the percent of trucks with the short, medium, and long axle spacing. An even distribution of 33, 33, and 34 percent for short, medium, and long axles, respectively, was used.

The percent of trucks is the axle spacing distribution of truck tractors (Class 8 and above). If other vehicles in the traffic stream also have the axle spacing in the range of the short, medium, and long axles defined above, the frequency of those vehicles was added to the axle-spacing distribution of truck tractors. For example, if 10 percent of truck traffic is from multiple trailers (Class 11 and above) that have the trailer-to-trailer axle spacing in the "short" range, 10 percent should be added to the percent trucks for "short" axles. Thus, the sum of percent trucks in the short, medium, and long categories can be greater than 100.

Input Processing

The traffic inputs are further processed to produce the following "processed input" for every month over the entire design period:

- Number of single axles under each load category.
- Number of tandem axles under each load category.
- Number of tridem axles under each load category.
- Number of quad axles under each load category.
- Number of truck tractors (Class 8 and above) under each load category (for top-down cracking).

The load combination for top-down cracking is assumed to consist of a steering axle and a tandem axle. The steering axle is assumed to have a fixed load of 12,000 lb, while the tandem axle is assumed to have the same load distribution as other tandem axles.

The hourly traffic distribution factors are applied to the processed traffic input (the traffic counts by axle type for every month of the design period) to obtain hourly traffic at the time of fatigue damage calculation for each distress.

Climate

Climate has a significant effect on the transverse cracking of JPCP. The interaction of the climatic factors with pavement materials and loading is complex. Factors such as solar radiation, cloud cover, precipitation, ambient temperature, and depth to water table affect pavement and subgrade temperature and moisture content, which, in turn, directly affects the layer moduli and ultimately the critical stresses involved. Also, temperature gradients through the concrete slab have a profound effect on cracking.

Climatic Inputs

The following weather related information is required for the cracking prediction.

- Hourly air temperature over the design period.
- Hourly precipitation over the design period.

- Hourly wind speed over the design period.
- Hourly percentage sunshine over the design period.
- Hourly ambient relative humidity values.
- Seasonal or constant water table depth at the project site.

The first five inputs above are obtained from weather station data for a given site, if available. For locations within the United States, they can be obtained from the National Climatic Data Center (NCDC) database. The Design Guide software includes an extensive climatic database for over 800 cities in the U.S. and a capability to interpolate between the available sites. All of the necessary climatic information at any given location within the U.S., with the exception of the seasonal water table depth, can be generated by simply providing the following inputs:

- Pavement location – latitude and longitude.
- Elevation.

Calibration used data from the closest weather station (called actual weather station [AWS]) or data interpolated from up to six closest weather stations (to create a virtual weather station [VWS]) at the specific pavement location. The VWS was used most often because the data are interpolated to the actual project location and this approach more adequately compensates for missing data from any one weather station.

Input Processing

The climatic inputs are combined with the pavement material properties, layer thicknesses, and drainage-related inputs by the EICM to yield the following information for use in the design analysis:

- Hourly profiles of temperature distribution through PCC slab—EICM produces temperatures at 11 evenly spaced points through slab thickness for JPCP analysis.
- Hourly temperature and moisture profiles (including frost depth calculations) through other pavement layers—obtained using EICM.
- Temperature at the time of PCC zero-stress temperature for JPCP design.
- Monthly or semi-monthly (during frozen or recently frozen periods) predictions of layer moduli for asphalt, unbound base/subbase, and subgrade layers.
- Annual freezing index values.
- Mean annual number of wet days.
- Number of freeze-thaw cycles.
- Monthly relative humidity values.

Effects of Climate on JPCP Cracking

Both temperature and moisture have a significant effect on the cracking of JPCP.

Temperature Difference from Solar Radiation

Temperature differences from top to bottom through the JPCP slab have a very significant effect on critical stresses at the top and bottom of the slab. On a hot sunny day, the top of the PCC slab is much warmer than the bottom (a positive temperature difference through the slab). The result is an elongation of the top of the slab relative to the bottom and a convex curvature, as shown in figure 5.

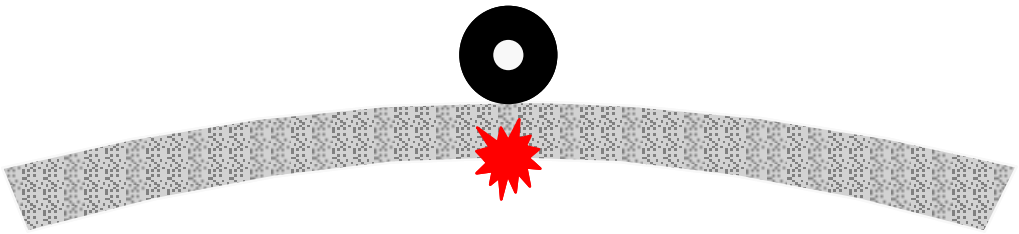

Figure 5. Curling of PCC slab due to daytime positive temperature difference plus critical traffic loading position resulting in high tensile stress at slab bottom.

Because self weight of the slab resists slab curling and because other factors cause the slab to curl upward, actual voids do no exist beneath the center of the slab.(3, 43) However, any forces (including self weight) that restrain free slab movements cause stress, and in this case, the restraint to slab curling results in increased tensile stress at the slab bottom. Under traffic loads, any actual loss of support due to temperature differences further increases the critical tensile stresses at the slab bottom.

During nighttime, the top of the PCC slab is typically cooler than the bottom (a negative temperature difference through the slab). This results in a concave curvature of the slab, as shown in figure 6. This is equivalent to having voids beneath the edges of the slab, which when combined with traffic load, increases tensile stress at the top that can lead to fatigue cracking initiating from top down.

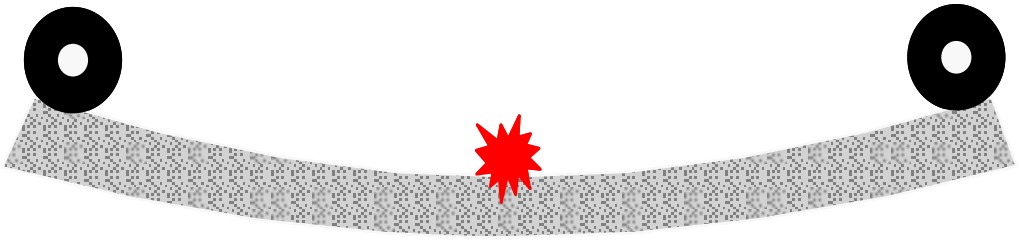

Figure 6. Curling of PCC slab due to nighttime negative temperature difference plus critical traffic loading position resulting in high tensile stress at slab top.

Because of the extreme sensitivity of critical stresses in JPCP to temperature gradients, consideration of hourly variation in temperature conditions is necessary. This is accomplished automatically using the EICM. Based on the hourly historical climatic data, pavement structure, and material properties, the EICM produces a file that includes historical hourly temperature profiles in the PCC slab for every year of the design period (8,760 profiles per design year [365 days * 24 hours]). An example of nonlinear temperature profiles through a 10 in PCC slab within a 24-hour period is shown in figure 7. The available climatic data are recycled to fill out the design period. For example, if the design period is 20 years, but only 5 years of climatic data are available, EICM determines the temperature profiles for the available 5 years, and then reuses the results 4 times to fill out the design period.

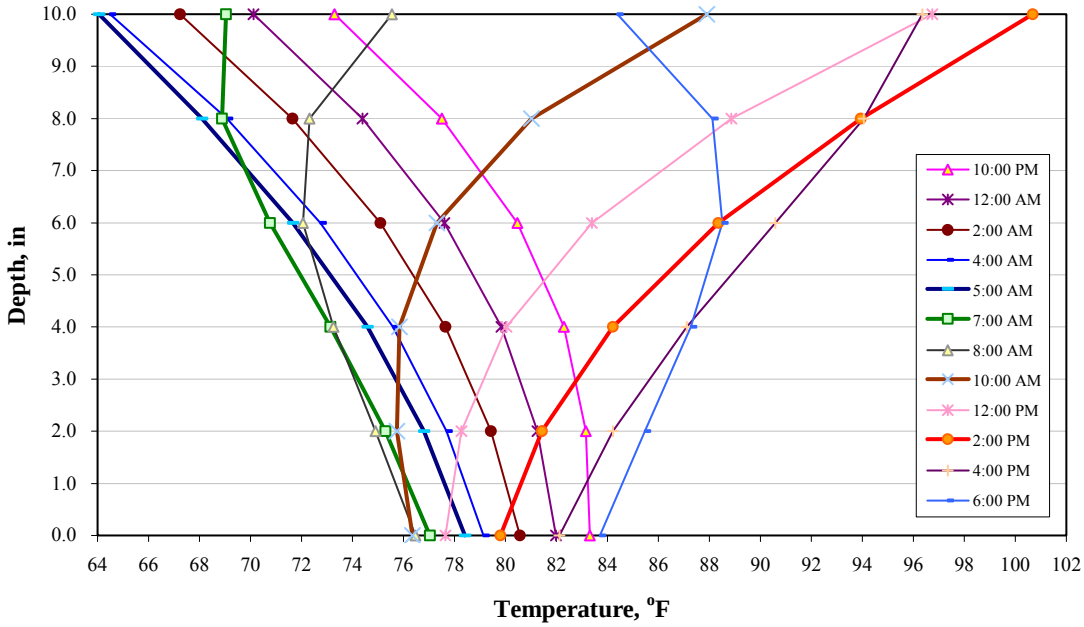

Figure 7. Example of temperature profile through a 10 in PCC slab for a typical spring day.

Each hourly nonlinear temperature profile is converted in the Design Guide software automatically to an effective linear temperature difference (difference) for computational efficiency. Using only the linear component (difference between temperatures at top and bottom of slab) can result in significant errors in estimating PCC stresses. These historical effective hourly temperature differences are use to create monthly daytime (positive) and nighttime (negative) temperature difference probability distributions for use in analysis.

Moisture Warping

Hardened concrete expands with an increase in moisture and contracts with a loss of moisture. The surface of PCC pavements can dry out, but below about the 2-inch level, the moisture level remains at a relatively constant high level (85 percent relative humidity or higher), even in very dry areas. This results in upward warping of the slab as shown in figure 6. The amount of drying shrinkage that takes place in the upper portion of the slab depends on many factors, including the type of curing, cement used, water content, and the PCC mix design.

A part of the drying shrinkage in PCC is irreversible, but there is a reversible portion that varies with the ambient relative humidity (*6, 7, 8*). The irreversible shrinkage causes the permanent moisture warping, while the reversible shrinkage causes seasonal variation in moisture warping (seasonal moisture warping) due to changes in ambient humidity.

Permanent Curling and Warping

PCC paving is often performed during the mornings of hot sunny days, a condition that tends to expose the newly paved PCC slabs to a high positive temperature difference from intense solar radiation plus the heat of hydration. The PCC slabs are flat when they harden, but depending on the exposure conditions a significant amount of positive temperature gradient (upper portion of the slab is much warmer than bottom) may be present at the time of hardening. This temperature has been termed the "built-in temperature gradient" or in this guide it is called the "zero-stress temperature gradient" (8, *9, 10, 11, 49*). Whenever the temperature gradient in the slabs fall below the amount locked into the slab at the time of construction (the zero-stress gradient), the slabs will attempt to curl upward causing tensile stress at the top of the slab which can lead to top down cracking of JPCP. Thus, an effective negative temperature gradient is permanently "built" into the slabs.

The upward curling of pavement slabs is restrained by several factors, including the slab self weight, dowels, and the weight of any base course bonded to the slab. This hypothesis has been supported using data from instrumented field slabs located in different climatic conditions (*8*). These factors affect the amount of actual permanent curl, as well as the amount of creep relaxation that may take place.

If the PCC paving is performed in the morning, the maximum heat of hydration and the maximum solar radiation coincides at about the same time resulting in a large built-in temperature gradient when the slab solidifies. If PCC paving is performed later in the afternoon or at night so that the highest temperature from the heat of hydration does not correspond with the most intense solar radiation, the amount of permanent temperature gradient "built" into the slab will be much lower and could potentially even be negative. Also, moist curing with water spray, wet burlap, or perhaps curing with reflective curing compounds can also produce a lower "zero-stress" or "built-in" permanent temperature gradient than regular curing compound.

As discussed under "Moisture Warping," differential moisture gradient causing a shrinkage gradient through the slab also produces a "permanent warping", which is superimposed on the zero-stress thermal gradient and is basically indistinguishable from permanent built-in curling. The permanent components of curling and warping are, therefore, considered together. The magnitude of permanent curling and warping is estimated from calibration of JPCP cracking and is expressed in terms of effective temperature difference from the top to bottom of the slab (called "permanent curl/warp"). It is important to note that only a portion of permanent curl/warp actually affects pavement response, because settlements that occur over time negate some of the effects of permanent curvature present in PCC slabs. The magnitude of permanent curl/ warp estimated from calibration reflects the effects of settlement into the base and creep.

Consideration of Climatic Effects in Cracking Prediction

The temperature and moisture effects are directly considered in the design of the JPCP as follows:

- The permanent built-in curling that occurs during construction (the zero-stress temperature gradient) is combined with the permanent warping due to differential shrinkage and expressed in terms of effective temperature difference between top and bottom (called "permanent curl/warp"). This parameter is a direct and influential input to the prediction of JPCP cracking.
- Transient hourly negative and positive temperature differences (from top to bottom of the slab) caused by solar radiation are computed using the EICM.
- Transient negative moisture shrinkage in the top of the slab caused by changes in relative humidity during each month of the year is converted to an equivalent temperature difference for every month.

All three of the above temperature and moisture differences through the PCC slab are predicted and appropriately combined along with axle loads to compute critical slab stresses, which are used within a monthly increment to accumulate damage at the bottom and at the top of the slab.

Permanent Curl/Warp Effective Temperature Difference

The magnitude of permanent curl/warp is a sensitive factor. Some of the factors that affect the permanent curl/warp include the following:

- Climate (air temperature, solar radiation, relative humidity, wind speed) during and after PCC placement.
- Construction time and curing procedure (morning construction with intense solar radiation, nighttime construction, regular curing compound, reflective curing compound, wet curing).
- PCC mix properties including cement type, water-cement ratio, cement quantity, and aggregate type.
- Creep of the PCC slab from self weight and edge constraints such as tied shoulder and doweled joints.
- Base stiffness (or the ability of slab to settle into the base to relieve curl/warp stresses).

Permanent Curl/Warp National Calibration

The actual slab curvature can be highly variable even along a given project, and a combination of adverse factors (e.g., a high shrinkage PCC mix, excessive temperature gradient at the time of PCC placement, and placement in morning hours and inadequate curing) can lead to extremely high permanent curl/warp, resulting in early top down cracking. A complete optimization analysis was conducted using the fatigue damage algorithm and the field cracking from over 500 observations. The goal was to select the permanent curl/warp that resulted in the lowest prediction error between measured and predicted cracking. The calibration results indicate that the values of long-term effective permanent curl/warp is fairly uniform, with no obvious bias based on climate or design factors, including slab thickness and base type. The recommended value for an effective linear permanent curl/warp is -10 °F from top to bottom of the slab for

JPCP for all climatic regions. This is an equivalent linear temperature difference from top to bottom of the slab.

Various design situations may occur where an increase or decrease in this parameter may be warranted. For example, nighttime construction should result in a lower value due to no solar radiation at night.(8, 50, 51) Another example identified during calibration of the JPCP cracking model indicated that when a significant amount of erosion occurs beneath a non-doweled transverse joint and loss of support occurs, an increased top down stress results. This often caused a transverse crack near the transverse joint on the leave side. Use of an increased value for permanent curl/warp (such as -15 °F) helps to account for this critical situation and predicts more accurately the amount of cracking that develops over time. Note that this situation could be handled in design through use of dowel bars and a more non-erodible base course.

PCC Materials

Portland Cement Concrete Layer

The PCC layer is not sub-layered for design and analysis purposes. The properties required for the PCC layer are divided into three categories—general and thermal properties, PCC mixture properties, and strength and stiffness properties.

General and Thermal Properties

- Layer thickness. The allowable range for design thickness is approximately 6 to 17 inches for new design.
- Poisson's ratio, μ – typical values for PCC range from 0.15 to 0.25.
- Coefficient of thermal expansion, α – PCC coefficient of thermal expansion can range from 4.1 to 7.3 x 10^{-6} / °F, depending on aggregate type. Determining this value through direct testing of the project mix (Level 1 input) is recommended.
- Thermal conductivity – the quantity of heat that flows normally across a surface of unit area per unit of time of temperature gradient normal to the surface. The recommended value is 1.25 BTU/hr-ft-°F.
- Heat capacity – the heat required to raise the temperature of a unit mass of material by a unit temperature. The recommended value is 0.28 BTU/lb-°F.

PCC Mix-Related Properties

The design procedure requires the following PCC mix-related inputs for modeling material behavior, including shrinkage, PCC zero-stress temperature, and load-transfer deterioration:

- Cement type – Types I, II, and III.
- Cement content.
- Water/cement ratio.
- Aggregate type.
- PCC zero-stress temperature, T_z – Defined as the temperature (after placement and during the curing process) at which the PCC layer exhibits zero thermal stress. If the PCC temperature is less than T_z, tensile stress occurs in the slab. The T_z is not actually a

single temperature but varies throughout the depth of the slab (termed a zero-stress gradient). However, when referring to T_z for purposes of joint and crack opening, it will be called simply the zero-stress temperature and could be considered as approximately the mean slab temperature. T_z can be input directly or can be estimated from monthly ambient temperature and cement content using the equation shown below, which is based on daytime construction and traditional curing compound.

$$T_z = (CC*0.59328*H*0.5*1000*1.8/(1.1*2400) + MMT) \qquad (1)$$

where,

T_z = temperature at which the PCC layer exhibits zero thermal stress (allowable range: 60 to 120 ^{0}F).
CC = cement content, lb/yd^3.
H = -0.0787+0.007*MMT-0.00003*MMT^2
MMT = mean monthly temperature for month of construction, ^{0}F.

Table 1 shows an illustration of the zero stress temperatures for different mean monthly temperatures and different cement contents in the PCC mix design. Note that the T_z equation has many limitations. It does not consider the effect of many factors on heat of hydration including mineral admixtures (flyash, slag), cement composition and fineness, chemical admixtures, and others. This equation was used in the calibration of JPCP and appeared to provide reasonable results.

- Ultimate shrinkage at 40 percent relative humidity – the ultimate shrinkage may be estimated using the equation presented in PART 2, Chapter 2. At input Level 1, this value needs to be determined through laboratory testing of the project mix.
- Reversible shrinkage – percent of ultimate drying shrinkage that is reversible upon rewetting. A value of 0.5 was used for the calibration.
- Curing method – curing compound or wet curing.

Table 1. Zero-Stress Temperatures based on PCC cement content and mean monthly ambient temperature during construction.

Mean Monthly Temperature	H	Cement Content lbs/cy			
		400	500	600	700
40	0.1533	52*	56	59	62
50	0.1963	66	70	74	78
60	0.2333	79	84	88	93
70	0.2643	91	97	102	107
80	0.2893	103	109	115	121
90	0.3083	115	121	127	134
100	0.3213	126	132	139	145

*Mean PCC temperature in degrees F.

Strength and Modulus Properties

The long-term strength gain of PCC, and corresponding change in PCC modulus, are required inputs. The PCC strength and modulus inputs consist of the following for JPCP:

- Modulus of rupture (flexural strength), MR.
- Static modulus of elasticity, E_{PCC}.
- Compressive strength, f'_c.

Depending on the input level, different amount of information is required as follows:

- Level 1—Laboratory values of MR, f'_c, f_t, and E_c at 7, 14, 28, and 90 days determined using appropriate testing procedures. The ratio of 20-yr to 28-day strength is also required. A best-fit regression line is fit through these data points to interpolate or extrapolate strength and stiffness at various ages during incremental damage calculation (see details in PART 2, Chapter 2). Very few of the JPCP sections had all of this input data.
- Level 2—Laboratory-determined values of compressive strength (f'_c) at 7, 14, 28, and 90 days and the 20-yr to 28-day strength ratio. The strength at each damage increment is determined using a best-fit regression line fit through these data points, and the remaining strength parameters (MR, f_t, and E_c) are estimated using well established strength-to-strength and strength-to-stiffness correlations (see PART 2, Chapter 2 for details). Very few of the JPCP sections used in calibration had this input data.
- Level 3—Estimated 28-day compressive strength or modulus of rupture from historical data or other information. The PCC strength over time is estimated using the default strength model, and the other inputs are calculated based on the projected strength using the appropriate correlations (see PART 2, Chapter 2 for details). The modulus of elasticity can also be input directly for Level 3 is desired. The large majority of JPCP sections for calibration used Level 3 estimation procedures to get this data. Most of the JPCP strength and modulus inputs were estimated by backcasting from core compression strength taken after several years of service. Some were based on specification requirements and other testing results from the agencies.

The processed input for PCC strength and stiffness properties varies month to month over the entire design period which was accomplished using the long term prediction model provided in Part II, Chapter 2.

Base Materials and Subgrade Soils

Three specific types of base layers (immediately beneath the slab) were considered. These include asphalt-stabilized, cement-stabilized, and unbound aggregates or soils.

Asphalt-Stabilized Base Layer

No sub-layering is done within the asphalt-stabilized base layer for rigid design and analysis. The materials inputs required for this layer are grouped under two broad categories – general materials inputs and inputs required to construct E^* master curve.

General Layer Property Inputs

- Layer thickness. Determined from core measurements.
- Poisson's ratio. Estimated based on default values for specific material types.
- Thermal conductivity – the quantity of heat that flows normally across a surface of unit area per unit of time of temperature gradient normal to the surface. The value for asphalt-stabilized base material is 0.67 BTU/hr-ft-°F.
- Heat capacity – the heat required to raise the temperature of a unit mass of material by a unit temperature. The value for asphalt-stabilized base is 0.23 BTU/lb-°F.
- Total unit weight – typical range for dense-graded hot-mix asphalt is 134 to 148 lb/ft^3. Obtained from cores cut from the pavement.

Inputs Required to Construct E Master Curve*

The primary material property of interest for asphalt stabilized layers is its dynamic modulus, E*. For Level 1 input, the dynamic modulus, E*, is determined in the laboratory using standard test protocols (see PART 2, Chapter 2 for details) for various frequencies and rates of loading. A master curve of E* versus reduced time is then derived from this data that defines the behavior of this layer under loading and at various climatic conditions. For input Levels 2 and 3, which was used to obtain E* for calibration sections, the dynamic modulus prediction equation presented in PART 2, Chapter 2 was used to construct the master curve from the following information:

Asphalt mixture properties (obtained from cores of sections or estimated based on typical values obtained from highway agency):

- Percent retained on ¾ in sieve – a typical value is 5 to 16 % for dense graded and 30% for permeable.
- Percent retained on 3/8 in sieve – a typical value is 27 to 49 % for dense graded and 70% for permeable.
- Percent retained on #4 sieve – a typical value is 38 to 61 % for dense graded and 95% for permeable.
- Percent passing the #200 sieve – a typical value is 3 to 8% for dense graded and 1% for permeable.

Asphalt binder – Level 1 input is generally not needed for rigid design (obtained from project specifications).

- For input Level 2 – specify PG grade or Viscosity grade.
- For input Level 3 – specify PG grade, Viscosity grade, or Penetration Grade.

Asphalt general (obtained from cores cut from the pavements)

- Volumetric effective binder content (percent).
- Air voids (percent).
- Reference temperature for master curve development (70 °F typical).

Chemically Stabilized Layers

No sub-layering is done for any cementitious stabilized base layers. The following inputs are required to define a cementitious stabilized layer:

Mean modulus of elasticity of the layer – this value is assumed to remain constant over the design period. The typical values for this input vary widely depending on material type and stabilizer content. Mean backcalculated values from all LTPP sites for two major types of cementitiously-stabilized bases are as follows. These values were used when core testing data were not available.

- Cement stabilized aggregate – mean modulus is 900,000 psi; range is 494,000 to 2,195,00 psi.
- Lean concrete – mean modulus is 2,099,000 psi; range is from 275,000 to 3,046,000 psi.
- Unit weight of the material.
- Poisson's ratio.
- Thermal conductivity – the value used for chemically or cementitiously stabilized base is 1.0 BTU/hr-ft-°F.
- Heat capacity – the value used for chemically or cementitiously stabilized base is 0.28 BTU/lb-°F.

Unbound Base/Subbase/Subgrade

The major inputs required for unbound base/subbase and subgrade layers are:

- Layer thickness (only for base and subbase layers) – for subgrade layers if the lime modified or compacted subgrades need to be considered separately from the natural subgrade, they can be defined as a structural layer.
- Layer resilient modulus.
- Poisson's ratio.
- Coefficient of lateral earth pressure, K_o – a typical value for unbound compacted materials is 0.5.

The layer resilient moduli for unbound layers and subgrade were estimated at two levels—Level 2 and Level 3. Level 2 required testing of a soil sample using some test such as CBR or R-value and then estimating the layer resilient modulus using a prediction equation. Level 3 required estimation using a correlation from soil classification such as AASHTO or UCS. A guide for selecting an appropriate Level 3 resilient modulus is provided in PART 2, Chapter 2. These resilient modulus values were used in the initial calibration run for each JPCP section. The resulting back calculated dynamic k value (obtained from the software as described next in this section) was then compared with that actually back calculated from the FWD testing on top of the JPCP slab. If the two dynamic k values were approximately the same as it was in many of the fine grained soils, no changes were made. If the field backcalculated k value was significantly lower or higher than the initial computer back calculated value, the resilient modulus of the subgrade was adjusted until they matched reasonably well.

It was found that whenever a granular subgrade existed, the recommended resilient modulus from PART 2, Chapter 2 is fairly high and if this subgrade layer is not truly infinite in depth, will result in overestimation of the subgrade support and a very high backcalculated k value (see section titled "Computation of Effective k-value"). If the stiffer granular layer is relatively thin (e.g., less than 5 to 10 ft) then a reduction in the selected subgrade resilient modulus is warranted as noted in PART 2, Chapter 2. However, the important aspect relative to calibration is that the

final resilient modulus used for any given JPCP subgrade was that which produced a back calculated k value that matched the field FWD backcalculated value. Thus, the stresses and deflections calculated in the analysis should be reasonable to those occurring in the actual pavement.

Seasonal Analysis

A seasonal analysis was used for all calibration sections with either Level 2 or Level 3 inputs. For Level 2, a representative design resilient modulus (at the optimum moisture content) or other allowable soil strength/stiffness parameters (CBR, R-value, AASHTO structural layer coefficient, or PI and gradation) was used and the EICM module linked to the Design Guide software estimates seasonal variations based on changing moisture and temperature profiles through the pavement structure. The additional inputs for EICM include plasticity index, percent passing No. 4 and No. 200 sieves, and the effective grain size corresponding to 60 percent passing by weight (D_{60}) for the layer under consideration. Using these inputs, EICM estimates the unit weight, the specific gravity of solids, saturated hydraulic conductivity of the pavement layer, optimum gravimetric moisture content, degree of layer saturation, and the soil water characteristic curve parameters. These computed quantities might be substituted with direct inputs. For Level 3, the layer resilient modulus at optimum water content was estimated and the EICM does the seasonal adjustment.

Sublayering of Unbound Layers and Subgrade

The original pavement structure defined by the user usually has four to six layers. However, the Design Guide software may internally subdivide the pavement structure into 12 to 15 sub-layers for the modeling of temperature and moisture variations. Only the unbound base layers thicker than 6 in and unbound subbase layer thicker than 8 in are sub-layered. For the base layer (first unbound layer), the first sub-layer is always 2 in. The remaining thickness of the base layer and any subbase layers that are sub-layered are divided into sub-layers with a minimum thickness of 4 in. For compacted and natural subgrades, the minimum sub-layer thickness is 12 in. A pavement structure is sub-layered only to a depth of 8 feet from the surface. Any remaining subgrade is treated as an infinite layer. If bedrock is present, the remaining subgrade is treated as one layer beyond 8 feet. Bedrock is not sub-layered and is always treated as an infinite layer.

The maximum number of layers that can be analyzed by the elastic layered analysis module is 20. This refers to the total number of sub-layers within the pavement structure, including any sub-layering done internally by the program. Note that the Design Guide software requires that an unbound material be designated as a "granular base" or "subgrade." If a pavement structure is input that includes one or more thick layers of unbound base material the sub-layering performed by the software may result in more than 20 layers which cannot be analyzed by the program. A message to this effect will appear on the screen and the user will have to modify the layering system. This can be done easily by reducing the thickness of the unbound base material and adding an identical material as a subgrade layer which is sub-divided into thicker sub-layers (e.g., an A-1-a granular base of 60 in could be transformed into a 24 in A-1-a base layer and 36 in A-1-a subgrade layer). Note that there can be as many "subgrade" layers as desired.

Bedrock

The presence of bedrock within 10 ft of the pavement surface influences the structural response of pavement layers. The inputs for this layer include the following:

- Unit weight.
- Poisson's ratio.
- Layer modulus.

Typical modulus values for bedrock in various conditions (e.g., solid, or highly fractured and weathered) are provided in PART 2, Chapter 2. Several of the calibration JPCP sections were suspected of having bedrock close to the surface and this was input for these cases.

Conversion of Layer Resilient Moduli to an Effective Dynamic Modulus of Subgrade Reaction

The subgrade and unbound pavement layers are characterized using resilient modulus in this Guide for all pavement types. For rigid pavement design, the subgrade k-value needed for the design analysis is obtained through a conversion process, which transforms the actual pavement structure into an equivalent structure that consists of the PCC slab, base, and an effective dynamic k-value, as shown in figure 8. This approach ensures that all pavement designs are accomplished using the same input for subgrade and other pavement layers. The "E-to-k" conversion is performed internally in the Design Guide software as a part of input processing.

Computation of Effective Dynamic k-Value

The effective dynamic k-value is obtained by first determining the deflection profile of the PCC surface using an elastic layer program (JULEA), modeling all layers specified for the design. The subgrade resilient modulus is adjusted to reflect the lower deviator stresses that typically exist under a concrete slab and base course as compared to the deviator stress used in laboratory resilient modulus testing. Next, the computed deflection profile is used to backcalculate the effective dynamic k-value. Thus, the effective dynamic k-value is a computed value, not a direct input to the design procedure (except in rehabilitation).

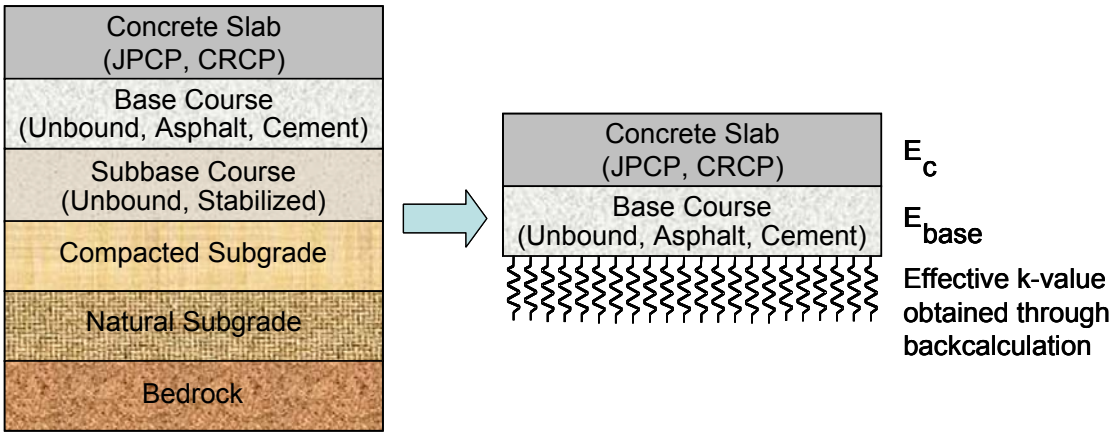

Figure 8. Structural model for rigid pavement structural response computations.

The effective k-value used in this Guide is a dynamic k-value, which should be distinguished from the traditional static k-values used in previous design procedures. The dynamic is twice that of the static k-value. The procedure to obtain the effective dynamic k-value for each time increment (month) is outlined in the following steps:

1. Assign layer parameters (E and Poisson's ratio) in a manner consistent with flexible pavement design (PART 3, Chapter 3).
2. Using the elastic layer program JULEA, simulate a 9,000-lb Falling Weight Deflectometer (FWD) load with the plate radius 5.9 in and compute PCC surface deflections at 0, 8, 12, 18, 24, 36, and 60 in from the center of the load plate.
3. Adjust the subgrade resilient modulus to account for the lowered deviator stress level beneath a PCC slab and base.
4. Using the elastic layer program JULEA, again simulate a 9,000-lb FWD load with the plate radius equal to 5.9 in, and with the recalculated subgrade resilient modulus and subbase moduli.
5. Calculate PCC surface deflections at 0, 8, 12, 18, 24, 36, and 60 in from the center of the load plate.
6. Use the Best Fit method (*12)* to compute the dynamic modulus of subgrade reaction using the PCC surface deflections.

The "effective" dynamic k-value represents the compressibility of all layers beneath the PCC slab. For example, if the pavement is constructed in a region with bedrock close to the surface (less than 10 ft), then the bedrock is entered as a stiff layer (high elastic modulus) beneath the subgrade soil layer. The PCC surface deflections calculated using JULEA reflects the presence of the bedrock layer; consequently, the presence of the bedrock layer is reflected in the calculated effective dynamic k-value.

The effective dynamic k-value of the subgrade is calculated for each month of the year and utilized directly to compute critical stresses and deflections in the incremental damage accumulation over the design life of the pavement. Factors such as water table depth, depth to bedrock, and frost penetration depth (frozen material) can significantly affect effective dynamic k-value. All of these factors are considered in the EICM.

Design Features

The transverse cracking prediction procedure allows a wide variety of PCC, base (layer directly underneath the PCC slab), and subbase material properties and layer thicknesses as shown in figure 9. For example, a rigid pavement structure could consist of a PCC slab, an asphalt treated base, an aggregate subbase, compacted subgrade, natural subgrade, and bedrock. The Design Guide software can be used to analyze a maximum of 20 layers; however, because of automatic sub-layering of certain layers a maximum of 10 actual input layers is recommended, comprising the pavement structure and subgrade (or bedrock). The following rules or constraints need to be satisfied in defining a rigid pavement structure for design:

- The surface layer in rigid pavement design is always a PCC layer.
- Slab-on-grade (two layers) is the minimum structure that can be analyzed.
- Only one unbound granular layer can be placed between two stabilized layers.

- The last two layers in the pavement structure must be unbound layers. To satisfy this constraint, the Design Guide software automatically sublayers the subgrade into two layers for slab-on-grade pavements and for pavements where a bound layer rests directly on the subgrade.

All pavement layers and material properties for each individual layer, including subgrade, were determined for the calibration sections. Depending on the section design, sub-layering may be necessary to satisfy the layering requirements of the analysis procedures. The Design Guide software performs the sub-layering internally based on the material type, layer thickness and the location of the layer within the pavement structure. More detailed guidelines on material properties are provided in detail in PART 2, Chapter 2.

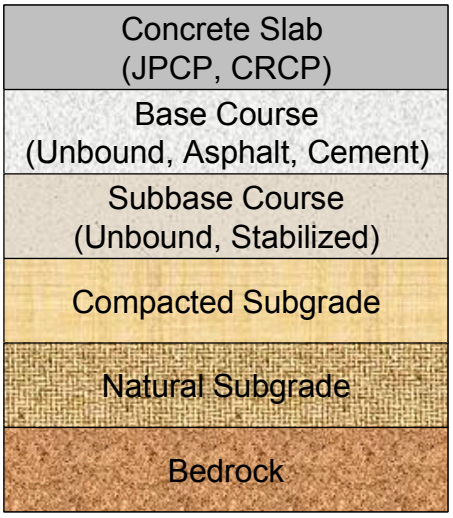

Figure 9. Illustration of JPCP pavement structure and layers capable of analysis.

3.0 STRUCTURAL RESPONSE MODEL

The structural response (bending stress used in transverse cracking) is based on the ISLAB2000 Finite Element Model (FEM). This model is described in Appendix QQ. This FEM was found to provide good accuracy of prediction of slab stresses and to be able to compute stress in a "reasonable" amount of time (i.e., computational practicality). The computer program ISLAB2000 is a major revision of the finite element program ILLI-SLAB that has been successfully used in rigid pavement analysis for many years. ISLAB2000 contains all positive features of ILLI-SLAB (including the features of ILSL2) but is free from several unnecessary limitations. The ISLAB2000 is able to model all of the important features of the pavement systems (multiple slabs in both directions, multiple layers, mismatched joints, multiple loads, temperature curling). A comparison of ABAQUS and ISLAB2000 models showed that the ISLAB2000 model, being significantly more computationally efficient, does not introduce significant error in the predicted structural responses. Comparisons of the stresses predicted by ISLAB2000 with the measured stresses from the AASHO Road test show good correspondence.

This structural model is capable of computing stresses for the following situations:

- Temperature and wheel loads – the model handled nonlinear temperature distribution in the PCC layer and multiple wheel loads.
- Loss of support due to slab curling (separation of PCC slab from foundation).
- The effects of base course – the model considers fully bonded and completely unbonded cases (either no slippage or free slippage between slab and base course, the version of ISLAB2000 that is currently available allows this capability but it was not available at the time this work was underway).
- Slab-to-slab interaction in a multiple slab system and load transfer across both transverse and longitudinal joints.

The stress calculations in the Design Guide software is accomplished using neural networks developed based on a large number of finite element analysis runs made using ISLAB2000. The ranges of input parameters covered in the neural networks are shown in table 2 for bottom-up stresses and in table 3.4.4 for top-down stresses. These ranges represent practical limits for each parameter.

The radius of relative stiffness listed in tables 2 and 3 is a composite parameter that represents the relative stiffness of the PCC slab with respect to foundation and is given by the following equation:

$$\ell = \sqrt[4]{\frac{E_{PCC} h_e^3}{12(1-\mu_{PCC}^2)k}} \qquad (2)$$

where,

$EPCC$	=	elastic modulus of PCC, psi.
h_e	=	effective slab thickness, in.
μ_{PCC}	=	PCC Poisson's ratio.
k	=	dynamic modulus of subgrade reaction (k-value), psi/in.

Table 2. Ranges of input parameters of the neural network for computing critical stresses at the bottom of PCC slab.

Input Parameter	Minimum Value	Maximum Value
Radius of relative stiffness [a]	22.5 in	80 in
Joint spacing	12 ft	30 ft [b]
Transverse joint LTE	0%	95%
Shoulder LTE	0%	90%
Axle offset from the slab edge	0 in	36 in
Wheel aspect (width-to-length) ratio	10	0.5
Temperature difference (top – bottom)	0 °F	> 40 °F [c]
Axle weight, single axle	0 lb	45,000 lb
Axle weight, tandem axle	0 lb	90,000 lb
Axle weight, tridem axle	0 lb	135,000 lb
Axle weight, quad axle	0 lb	135,000 lb
Tandem and tridem axle spacing	40 in	70 in

[a] The radius of relative stiffness of highway pavements typically fall between 22.5 and 80 in. Analyses based on plate theory become increasingly inaccurate for the radius of relative stiffness values beyond the limit shown above.

[b] For typical highway pavements the bottom-up stress reaches the maximum value at joint spacing less than 30 ft. The results for 30-ft slab are given for the actual joint spacing greater than 30 ft. In general, long joint spacing (20 ft or greater) is not recommended because of excessive curling stress.

[c] Depends on PCC coefficient of thermal expansion, k-value, PCC unit weight, PCC thickness, and radius of relative stiffness.

Table 3. Ranges of input parameters of the neural network for computing critical stresses at the top of PCC slab.

Input Parameter	Minimum Value	Maximum Value
Radius of relative stiffness [a]	22.5 in	80 in
Joint spacing	12 ft	20 ft [b]
Transverse joint LTE	50% if nondoweled 85% if doweled	
Shoulder LTE	0%	90%
Axle offset from the slab edge	0 in	36 in
Wheel aspect (width-to-length) ratio	10	0.5
Temperature difference (top – bottom)	0 °F	< -80 °F [c]
Wheelbase	12 ft	20 ft
Axle weight, single axle	Fixed at 12,000 lb	
Axle weight, tandem axle	0 lb	135,000 lb
Tandem axle spacing	40 in	70 in

[a] The radius of relative stiffness of highway pavements typically fall between 22.5 and 80 in. Analyses based on plate theory become increasingly inaccurate for the radius of relative stiffness values beyond the limit shown above.

[b] For typical highway pavements, the top-down stress is close to the maximum value when the joint spacing reaches 20 ft. The results for 20-ft slabs are given for the actual joint spacing greater than 20 ft. In general, long joint spacing (e.g., 20 ft or greater) is not recommended because of excessive curling stress.

[c] Depends on PCC coefficient of thermal expansion, k-value, PCC unit weight, PCC thickness, and radius of relative stiffness.

The incremental design procedure adopted in this Guide requires hundreds of thousands of stress and deflection calculations to compute monthly damage (for the different loads, load positions, and equivalent temperature differences) over a design period of many years. These computations would take days to complete using existing finite element programs. To reduce computer time to a practical level, neural networks (NNs) have been developed, based on the ISLAB2000 finite element (FE) structural model (*1*), to accurately compute critical stresses and deflections virtually instantaneously. This makes it possible to conduct detailed, month-by-month, incremental analysis within a practical time frame (within a few minutes). A series of neural networks were developed for different analyses that accurately reproduce the results given by direct FE analysis (R^2 of 0.99). Appendix QQ provides a detailed description of the finite element models and neural networks.

4.0 INCREMENTAL DAMAGE ALGORITHM

Fatigue damage at critical points in the PCC slab is accumulated in an incremental manner, month by month over the analysis period. As the fatigue damage becomes larger and larger the "weakest" slabs along the project begin to show transverse or diagonal cracking. For example, these slabs could have less than average thickness, strength, or support; or higher than average thermal coefficient of expansion. As traffic loading and climatic gradients continue, fatigue damage increases and additional slabs develop cracking until at some point it is determined necessary to perform a structural overlay.

This section provides the step-by-step procedure used to accumulate damage that leads to transverse cracking of JPCP calibration sections. The steps are as follows.

1. Tabulate input data – summarize all inputs needed for predicting JPCP cracking.
2. Process traffic data – the processed traffic data needs to be further processed to determine equivalent number of single, tandem, and tridem axles produced by each passing of tandem, tridem, and quad axles.
3. Process pavement temperature profile data – the hourly pavement temperature profiles generated using EICM (nonlinear distribution) need to be converted to distribution of equivalent linear temperature differences by calendar month.
4. Process monthly relative humidity data – the effects of seasonal changes in moisture conditions on differential shrinkage is considered in terms of monthly deviations in slab warping, expressed in terms of effective temperature difference.
5. Calculate stress – calculate stress corresponding to each load configuration (axle type for bottom-up and axle spacing for top-down), load level, load position, and temperature difference for each month within the design period.
6. Calculate fatigue damage – calculate damage for each damage increment and sum to determine total bottom-up and top-down damage over the entire life of each calibration section where slab cracking data were available.
7. Observed slab cracking was plotted versus fatigue damage to obtain a calibrated cracking model.

Assumptions

The following were assumed in the fatigue analysis:

- Linear damage accumulation – the procedure is based on Miner's hypothesis (*22*).
- The pavement structure is modeled as a two-layered system consisting of slab and base with either a bonded or unbonded interface. The effects of subbase layers, as well as the shear contribution of the base layer, are accounted for through the use of effective dynamic modulus of subgrade reaction.
- Lateral traffic wander is modeled as a normal distribution using mean wheelpath and standard deviation.
- The stresses in JPCP at the pavement edge do not immediately drop off to an insignificant level when the traffic wheel goes partially off the pavement. The effects of wheels placed x inches outside of the pavement edge is assumed equal to those placed x inches inside of the pavement edge. Thus, the probability of traffic wheel being $-x$ in and $+x$ in from the pavement edge are added together for damage calculation, as illustrated in figure 10.

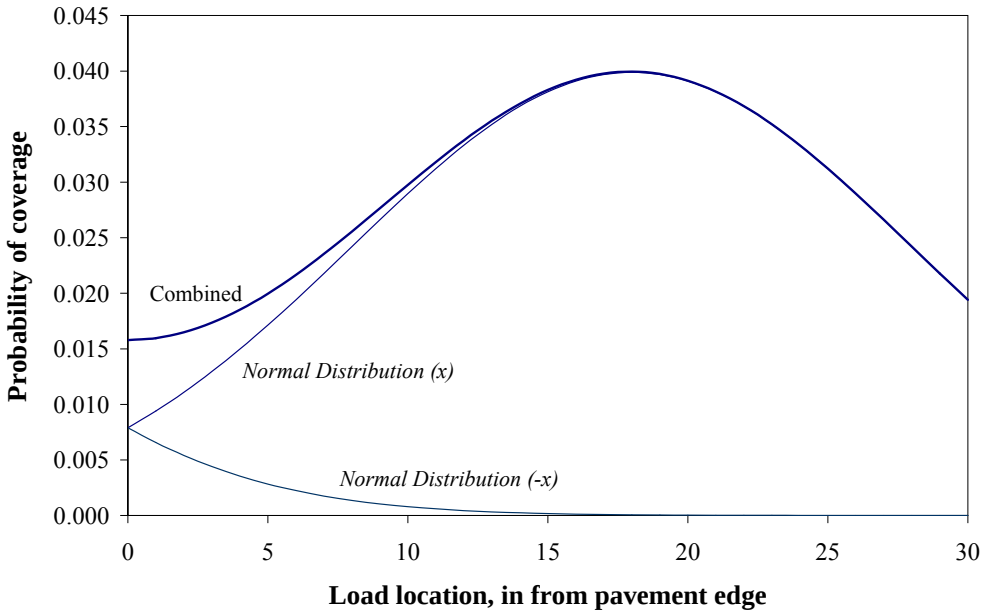

Figure 10. Illustration of probability of coverage including the effects of the axle load being partially off of the pavement.

The use of widened slab design is assumed to change the critical damage location for fatigue damage from the lane-shoulder edge to the longitudinal lane-to-lane joint edge. Therefore, the effects of widened slabs (in terms of fatigue cracking) are similar to those of tied PCC shoulder, except that there is a further benefit of the mean wheelpath being further from the critical edge, which effectively reduces the number of critical load applications. If the mean wheelpath is measured from the paint stripe at the lane-shoulder edge to the outer edge of the wheel, the effective mean wheelpath for widened slab design is as follows:

$$x^* = LW - AW - x \quad (3)$$

where,

x^* = effective mean wheelpath, in.
LW = lane width, in. Typical lane width is 12 ft (144 in).
AW = axle width measured from the outer edge to outer edge of axle, in. Typical axle width is 8.5 ft (102 in).
x = mean wheelpath measured from the paint stripe to the outer edge of tire, in.

For example, if the mean wheelpath for widened slab design is 18 in (measured from the paint stripe to the outer edge of outermost tire closest to the paint stripe) and axle width is 8.5 ft (102 in), the effective mean wheelpath is 24 in.

- Base Poisson's ratio is equal to PCC Poisson's ratio.
- Base coefficient of thermal expansion is equal to PCC coefficient of thermal expansion.
- Temperature distribution through the base layer is constant.

Steps Used To Calibrate Transverse Cracking

The following steps were performed for every JPCP calibration section.

Step 1: Tabulate input data

Tabulate all input required for JPCP cracking prediction. The required parameters are summarized in table 4. In addition to the inputs listed in this table, the processed inputs from Steps 2, 3, and 4 below are needed for the fatigue analysis of JPCP.

Step 2: Process traffic data.

The traffic inputs are first processed to determine the expected number of single, tandem, tridem, and quad axles in each month within the design period. This procedure is described in detail in PART 2, Chapter 4. For bottom-up damage, each passing of an axle may cause one or more occurrences of critical loading. Each passing of an axle is converted to an equivalent number of single, tandem, or tridem axles for bottom-up damage computation for different axle types as shown in figure 11:

One actual single axle is effectively equal to one application of a single axle of the same load (figure 11a).
One actual tandem axle is effectively equal to two applications of a tandem axle of the same load at the positions shown in figure 11b.
One actual tridem axle is effectively equal to one tridem axle of the same load and two tandem axles with two-thirds the total load (figure 11c).

One actual quad axle is effectively equal to two tridem axles with three-fourths the total load and two tandem axles with half the total load (figure 11d).

For top-down cracking, the number of loadings by short, medium, and long wheel base trucks (or axle combinations) is determined by multiplying the total number of trucks by the percentages of short, medium, and long wheel base trucks. For both bottom-up and top-down cracking, the

hourly traffic is calculated by multiplying the monthly load applications by the hourly truck traffic distribution factors.

Step 3: Process temperature profile data

The EICM produces temperatures at 11 evenly spaced points through the thickness of the PCC layer. For calculation expediency, each temperature profile is converted to equivalent linear temperature difference (top minus bottom), and the frequency distribution of the equivalent linear temperature difference is determined for each calendar month as follows:

Table 4. Summary of input parameters for JPCP cracking prediction.

Input	Variation*	Source
Design life (yr)	Fixed	Direct design input
Month of project opening	Fixed	Direct design input
PCC age at opening (mo)	Fixed	Direct design input
PCC strength for each month (psi)	Design mo[1]	Result of PCC strength input processing (section 3.4.3.6 *Pavement Structure Input*)
PCC modulus for each month (psi)	Design mo[1]	
Joint Spacing (ft)	Fixed	Direct design input
Dowel diameter (in)	Fixed	Direct design input
Loss of bond age (mo)	Fixed	Direct design input
Lane-shoulder deflection LTE (%)	Fixed	Direct design input
Widened slab (yes/no)	Fixed	Direct design input
Poisson's ratio	Fixed	Direct design input
PCC unit weight (pcf)	Fixed	Direct design input
Coefficient of thermal expansion (/°F)	Fixed	Direct design input
Ultimate reversible shrinkage strain (10^{-6})	Fixed	Direct design input or calculated value based on PCC mix properties
Time to 50% ult. Shrinkage (days)	Fixed	Direct design input
Base thickness (in)	Fixed	Direct design input
Base unit weight (pcf)	Fixed	Direct design input
Monthly base modulus (psi)	Calendar mo[2]	Result of Seasonal Analysis (section 3.4.3.6 *Pavement Structure Input*)
Monthly effective subgrade k-value (psi/in)	Calendar mo[2]	Results of "E-to-k" conversion (section 3.4.3.6 *Pavement Structure Input*)
Permanent curl/warp (°F)	Fixed	Direct design input
Edge-to-edge (outside) axle width (ft)	Fixed	Direct design input
Lane width (ft)	Fixed	Direct design input
Mean wheelpath (in)	Fixed	Direct design input
Traffic wander standard deviation (in)	Fixed	Direct design input
Slab width (ft)	Fixed	Direct design input
Tire pressure (psi)	Fixed	Direct design input
Axle spacing (in)	Fixed	Direct design input
Dual wheel spacing (in)	Fixed	Direct design input
Tire width (in)	Fixed	Direct design input
Wheelbase – short, medium, and long (ft)	Fixed	Direct design input
% trucks at each wheelbase (%)	Fixed	Direct design input

[1] Design mo: parameters that vary with pavement age; [2] Calendar mo: parameters that vary seasonally.

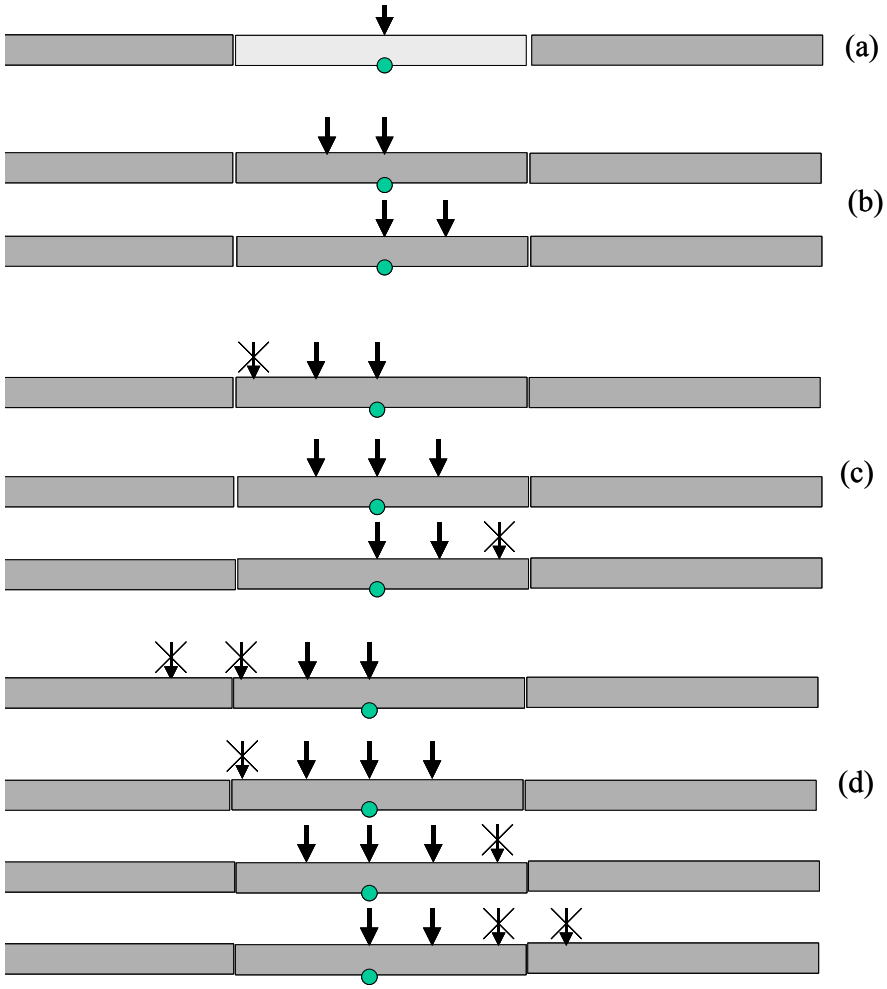

Figure 11. Accounting for different axle types in JPCP bottom-up cracking damage accumulation: (a) single, (b) tandem, (c) tridem, and (d) quad axles.

1. Establish a table of temperature difference verses corresponding stress in 2 °F increments with the following loads placed at the pavement edge:
   - Bottom-up stress – 18,000-lb single axle. The axle should be placed halfway between the transverse joints to produce the maximum stress.
   - Top-down stress – a single-tandem axle combination with 12,000 lb on the single axle and 34,000 lb on the tandem. Use the medium wheelbase, and position the axles to produce maximum stress. A critical loading condition for top down stress is illustrated in figure 2.
2. Determine the stress corresponding to the actual nonlinear temperature profile and the same wheel loads used in step 1 above (*23*). Prior to running stress analysis, the permanent curl/warp should be applied to each actual temperature profile so that the combined stress will be determined with the correct contact condition.
3. Look up the table created in step 1 to determine the equivalent linear temperature difference corresponding to each of the actual temperature case analyzed in step 2 based on stress equivalence.

4. Summarize the equivalent linear temperature difference by calendar month to obtain the frequency distribution of hourly temperature differences as follows:
   - Frequency distribution of positive temperature differences – all temperature profiles that produce a positive temperature difference (top warmer than bottom) is compiled together to determine the temperature frequency distribution for bottom-up cracking.
   - Frequency distribution of negative temperature differences – all temperature profiles that produce a negative temperature difference (top cooler than bottom) is compiled together to determine the temperature frequency distribution for top-down cracking.

   The temperature-difference frequency distributions are determined for each month of the year to coordinate with the input variations that are considered on monthly basis (e.g., base stiffness, effective subgrade k-value, and moisture warping).

The equivalent linear temperature-difference frequency distributions are based on hourly temperature profiles; thus, the fatigue damage calculation, in effect, is performed on hourly basis.

Step 4: Process monthly relative humidity data

Moisture warping is adjusted monthly based on atmospheric relative humidity. The effects of monthly variation in moisture warping are expressed in terms of equivalent temperature difference and are added to the equivalent linear temperature difference during stress calculations.

$$ETG_{SHi} = \frac{3 \cdot (\varphi \cdot \varepsilon_{su}) \cdot (S_{hi} - S_{h\,ave}) \cdot h_s \cdot \left(\frac{h}{2} - \frac{h_s}{3}\right)}{\alpha \cdot h^2 \cdot 100} \qquad (4)$$

where,

ETG_{Shi} = temperature difference equivalent of the deviation of moisture warping in month *i* from the annual average, °F.

φ = reversible shrinkage factor, fraction of total shrinkage. Use 0.5 unless more accurate information is available.

ε_{su} = ultimate shrinkage (ε_{su} may be estimated based on PCC mix properties using the equation presented in PART 2, Chapter 2), x 10^{-6}:

S_{hi} = relative humidity factor for month *i*:

$$S_{hi} = 1.1 \cdot RH_a \qquad \text{for } RH_a < 30\%$$
$$S_{hi} = 1.4 - 0.01 \cdot RH_a \qquad \text{for } 30\% < RH_a < 80\% \qquad (4a)$$
$$S_{hi} = 3.0 - 0.03 \cdot RH_a \qquad \text{for } RH_a \geq 80\%$$

RH_a = ambient average relative humidity, percent

Sh_{ave} = annual average relative humidity factor. Annual average of Shi.

h_s = depth of the shrinkage zone (typically 2 in).

h = PCC slab thickness, in.

α = PCC coefficient of thermal expansion, /°F.

The temperature-difference equivalent of the monthly deviations in moisture warping (ETG_{Shi}) given by equation 4 is based on ultimate shrinkage, which takes time to develop. The ETG_{Shi} at any time t days from placement is

$$ETG_{SHt} = S_t \cdot ETG_{SHi} \tag{5}$$

where,

ETG_{Shi} = ETG_{Shi} at any time t days from PCC placement, °F.
ETG_{Shi} = temperature difference equivalent of the deviation of moisture warping in month i from the annual average, °F.

$$S_t = \frac{Age}{n + Age} \tag{6}$$

S_t = time factor for moisture-related slab warping.
Age = PCC age, days since placement.
n = time to develop 50% of ultimate shrinkage strain, days. Use 35 (the ACI recommended value), unless more accurate information is available (6).

Step 5: Calculate stress

Calculate stress for all cases that needs to be analyzed. The number of cases depends on the damage increment. For JPCP transverse cracking calibration, the following increments are considered:

- Pavement age – by year.
- Season – by month.
- Load configuration – axle type for bottom-up cracking; wheelbase for top-down cracking.
- Load level – discrete load levels in 1,000 to 3,000 lb increments, depending on axle type.
- Temperature gradient – equivalent linear temperature difference from top to bottom in 2 °F increments.
- Lateral load position – 6 specific locations for both top-down and bottom-up cracking.

The damage increments and stress calculation were discussed earlier in this section.

Step 6: Calculate fatigue damage

As discussed earlier, all cases that produce significantly different stresses must be evaluated separately in the Miner's fatigue analysis (as a separate damage increment) to obtain accurate results. The general expression for fatigue damage accumulations considering all critical factors for JPCP transverse cracking is as follows:

$$FD = \sum \frac{n_{i,j,k,l,m,n}}{N_{i,j,k,l,m,n}} \tag{7}$$

where,

FD = total fatigue damage (top-down or bottom-up).

$n_{i,j,k,\ldots}$ = applied number of load applications at condition *i, j, k, l, m, n*.
$N_{i,j,k,\ldots}$ = allowable number of load applications at condition *i, j, k, l, m, n*.
i = age (accounts for change in PCC modulus of rupture, layer bond condition, deterioration of shoulder LTE).
j = month (accounts for change in base and effective dynamic modulus of subgrade reaction).
k = axle type (single, tandem, and tridem for bottom-up cracking; short, medium, and long wheelbase for top-down cracking).
l = load level (incremental load for each axle type).
m = temperature difference.
n = traffic path.

The damage increments were discussed previously in this section.

The applied number of load applications ($n_{i,j,k,l,m,n}$) is the actual number of axle type *k* of load level *l* that passed through traffic path *n* under each condition (age, season, and temperature difference). The allowable number of load applications is the number of load cycles at which fatigue failure is expected (corresponding to 50 percent slab cracking) and is a function of the applied stress and PCC strength. The allowable number of load applications is determined using the following field calibrated fatigue model:

$$\log\left(N_{i,j,k,l,m,n}\right) = C_1 \cdot \left(\frac{MR_i}{\sigma_{i,j,k,l,m,n}}\right)^{C_2} + \quad 0.4371 \tag{8}$$

where,

$N_{i,j,k,\ldots}$ = allowable number of load applications at condition *i, j, k, l, m, n*
MR_i = PCC modulus of rupture at age *i*, psi
$\sigma_{i,j,k,\ldots}$ = applied stress at condition *i, j, k, l, m, n*
C_1 = calibration constant = 2.0
C_2 = calibration constant = 1.22

The fatigue damage calculation is a simple process of summing damage from each damage increment, except that a numerical integration scheme is used to accurately determine the effects of traffic wander. The fatigue damage at the critical damage location caused by an axle load placed at any random distance away from the pavement edge (point *j*) is given by the following:

$$FD^*_{ij} = P\left(COV_j\right) \cdot FD_{ij} \tag{9}$$

where,

$FD^*_{ij.}$ = fatigue damage at location *i* (critical damage location) due to the fraction of total applied traffic passing through point j.
$P(COV_j)$ = probability of traffic passing through point *j*.
$FD_{ij.}$ = fatigue damage at location *i* (critical damage location) due to the traffic load passing through point j.

The probability of coverage is determined assuming normal distribution.

$$NORMDIST = \frac{1}{SD_{traf}\sqrt{2\pi}} e^{-\frac{1}{2}\left(\frac{x-\mu}{\sigma}\right)^2} \quad (10)$$

where,

NORMDIST = normal distribution density function.
x = wheel location – distance from pavement edge (or outside of the paint stripe for widened slab) to the outer edge of outermost wheel, in.
μ = mean wheel location, in.
SD_{traf} = traffic wander standard deviation, in.

The fatigue damage contribution due to traffic passes at different distances from the pavement edge is illustrated in figure 12. The total fatigue damage due to all traffic passes is obtained by summing damage caused by traffic passing through all traffic paths. This is simply the area under the curve shown in figure 12. The area under the curves can be calculated in thin strips (approximating the area for each strip as a trapezoid), but more accurate results can be obtained more efficiently using numerical integration methods. The Gauss integration method is used for the JPCP cracking model. Using the Gauss numerical integration scheme outlined below is equivalent to analyzing stresses using infinitesimally small load position increments. In this method, the value of the function evaluated at prescribed locations and the associated weighting factors are used to determine the area under polynomial functions as follows:

$$\int_a^b f(x)\,dx = A \cdot \sum_{i=0}^{n} f(x_i) \cdot w(x_i) \quad (11)$$

where,

$f(x)$ = function being integrated.
A = scaling factor, width of traffic channel that produces significant fatigue damage (20 in for bottom-up cracking; 40 in for top-down cracking).
$f(x_i)$ = function value at normalized location x_i (-1 to 1) (equation 7).
$w(x_i)$ = weighting factor for the function value at normalized location x_i (-1 to 1).

The Gauss integration method integrates polynomials of order 2n-1 exactly, where n is the number of evaluation points used. For both the JPCP cracking model and the CRCP punchout model, the integration is performed in two pieces, because the relative fatigue damage contribution curves (e.g., figure 12) can have a very high gradient near the pavement edge but are typically very flat at distances away from the edge. A single polynomial function does a poor job of fitting curves that contains both a region of very high gradient and a flat portion. Therefore, 4-point Gauss integration is used for outer strip, and 2-point Gauss integration is used for the interior portion. The specified evaluation points and weighting factors for 2- and 4-point Gauss integration are as follows:

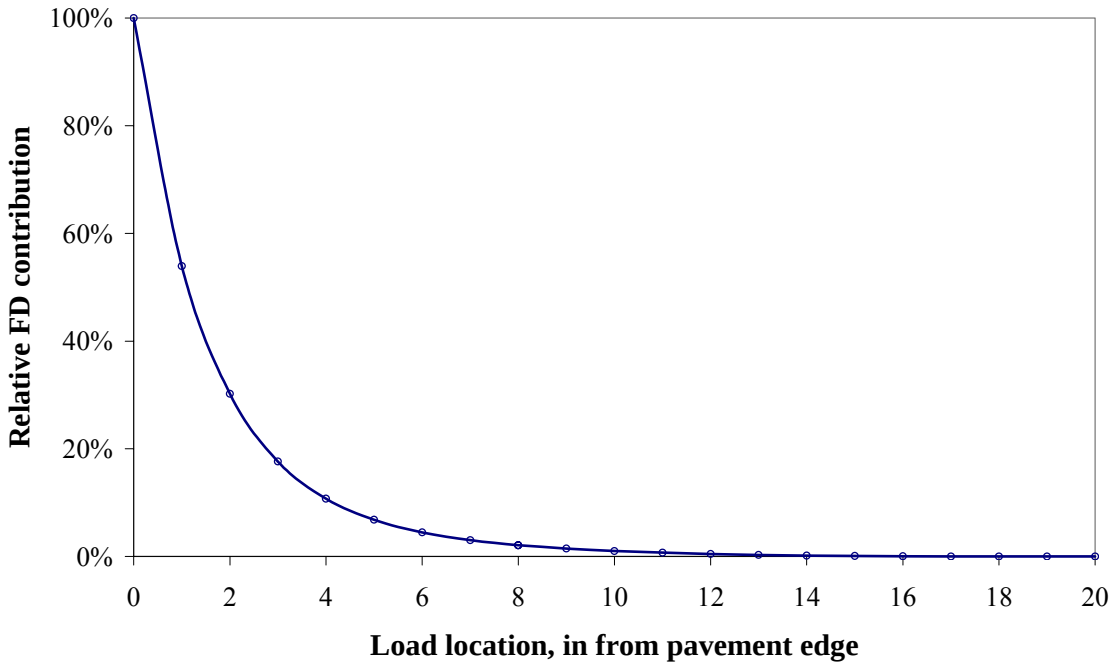

Figure 12. Illustration of fatigue damage contribution by traffic passes at various distances from the pavement edge.

2-point Gauss integration:

- Evaluation point: $\pm\frac{1}{\sqrt{3}}$ Weighting factor: 1

4-point Gauss integration:

- Evaluation point: $\pm\sqrt{\frac{3+2r}{7}}$ Weighting factor: $\frac{1}{2}-\frac{1}{6r}$
- Evaluation point: $\pm\sqrt{\frac{3-2r}{7}}$ Weighting factor: $\frac{1}{2}+\frac{1}{6r}$

$r=\sqrt{1.2}$

For bottom-up cracking in JPCP, the following integration scheme was used:

Total width of traffic path considered: 20 in.
Outer 8-in strip: 4-point Gauss integration.

- Gauss points: 0.5555, 2.640, 5.360, and 7.445 in from slab edge.
- Weighting factors: 0.34785, 0.65215, 0.65215, and 0.34785, listed in the order of the Gauss points listed above.

Remaining interior 12-in strip: 2-point Gauss integration.

- Gauss points: 10.54, and 17.46 in from slab edge.
- Weighting factors: 1.0 and 1.0.

For top-down cracking in JPCP, the following integration scheme was used:

Total width of traffic path considered: 40 in.
Outer 8-in strip: 4-point Gauss integration.

- Gauss points: 1.666, 7.920, 16.080, and 22.334 in from slab edge.
- Weighting factors: 0.34785, 0.65215, 0.65215, and 0.34785, instead in the order of the Gauss points listed above.

Remaining interior 12-in strip: 2-point Gauss integration.

- Gauss points: 27.381, and 36.619 in from slab edge.
- Weighting factors: 1.0 and 1.0.

The stresses calculated for the six Gauss points under each pavement age, month, axle type, axle load, and temperature difference are used to calculate damage considering traffic wander under each combination of conditions. The process is repeated for the entire factorial of these parameters (pavement age, month, axle type, axle load, and temperature difference) and the calculated damage for each condition summed to determine the total damage. The same procedure is used for bottom-up and top-down damage calculation.

5.0 CALIBRATION OF DAMAGE/CRACKING MODEL

The damage calculated and accumulated as described in Section 4.0 is a mechanistic parameter that represents a relative index of load associated damage within the pavement structure. When "damage" is very small (e.g., 0.00001) the pavement structure would not be expected to have any physical cracking. If slab cracking does exist this may be caused by construction problems and not from repeated load fatigue damage. As computed "damage" increases to a significant value (e.g., 0.1 or greater), actual cracking may be expected to develop in a few locations along the project.

Field JPCP Sections Used in Calibration

The JPCP transverse cracking model was calibrated based on performance of 196 field sections located in 24 States as shown in figure 13. The calibration sections consist of LTPP GPS-3 and SPS-2 JPCP sections and 36 JPCP sections from the FHWA study *Performance of Concrete Pavements* (*2*). Time-series data were available for many of the sections, making the total number of field cracking observations 516. The required inputs for each of these sections are provided in Appendix FF. Table 5 was assembled to show some general information about the JPCP sections. The collection of many inputs for each section that are required to drive the cracking fatigue damage model was a major work effort and required a huge amount of time and resources. For example, the field collection data sheets were examined for every section to ensure that transverse cracking was properly recorded and also to obtain cracking for each of the joint spacings where random spacing existed on a JPCP section. This provided much expanded data on the effect of joint spacing at a given site. There were many missing data elements which caused the deletion of several JPCP sections (e.g., mostly missing traffic and materials data).

The JPCP sections were generally under heavy truck traffic as shown in figure 14 which gives the distribution of the number of total heavy trucks (class 4 and above) typically in the outer lane. The number of trucks ranges over 20 million (ESALS up to 30 million). The age of these sections range up to 34 years as shown in figure 15.

Figure 13. Map showing States with the number of JPCP sections used in calibration of the slab cracking model.

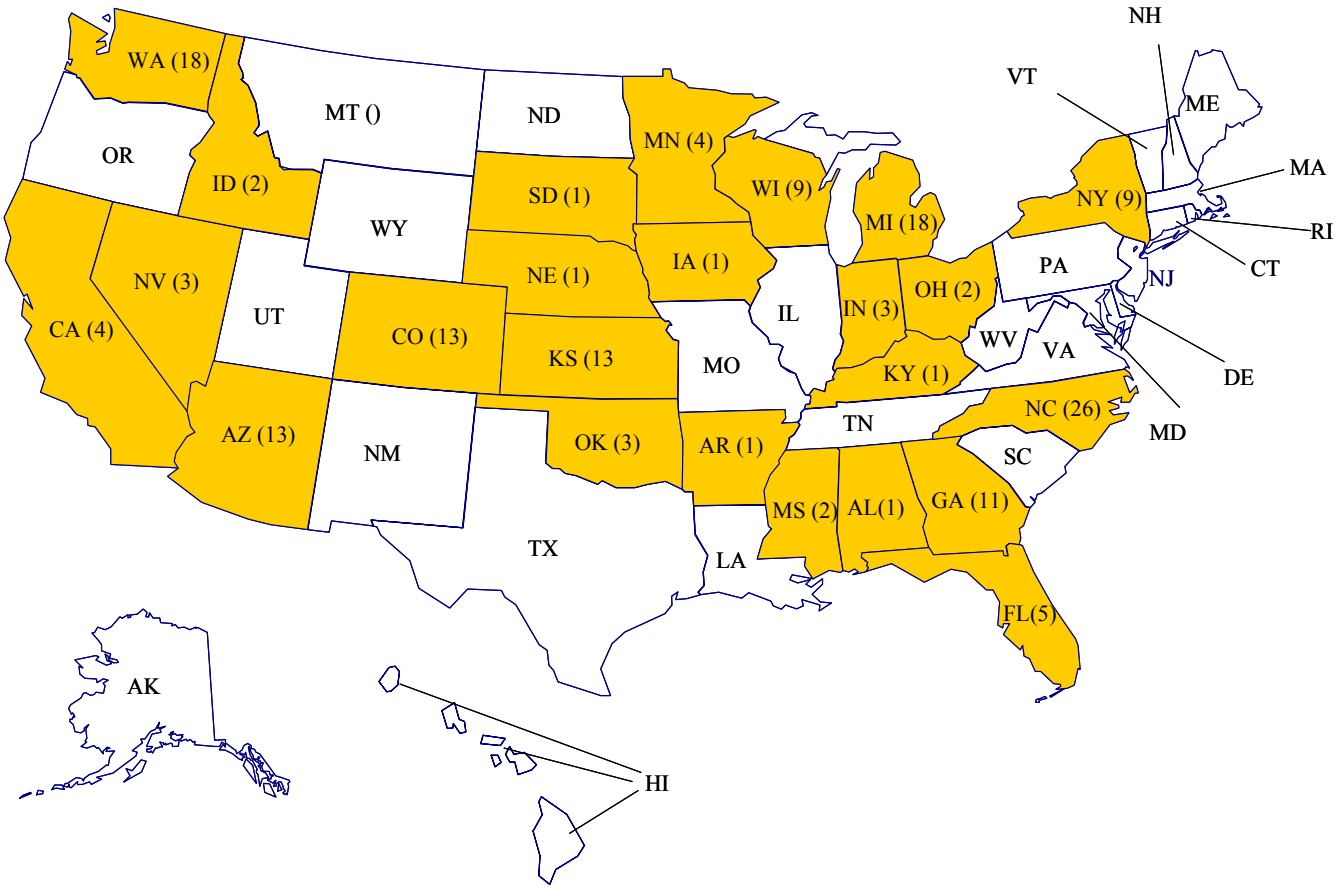

Table 5. Summary of general information and site/project identification information for the projects used in New J and calibration (obtained from LTPP GPS-3 and SPS-2 and FHWA RPPR).

SHRP_ID	State	County	Functional Class	Route Signing	Route No.	Direction of Travel	Mile Point	Section Length, ft	Const. Month
1_3028	Alabama	Jefferson	UPA- Interstate	Interstate	59	North	138.1	500	6
12_3811	Florida	Gadsden	RPA- Interstate	Interstate	10	West	187.1	500	2
12_4000	Florida	Volusia	RPA- Other	U.S. Highway	92	East	4.48	500	11
12_4057	Florida	Hillsborough	RPA- Interstate	Interstate	75	South	256.33	500	6
12_4109	Florida	Volusia	RPA- Other	U.S. Highway	1	South	11.37	500	3
12_4138	Florida	Volusia	RPA- Other	U.S. Highway	92	East	9.59	500	11
16_3017	Idaho	Power	RPA- Interstate	Interstate	86	East	24.72	500	9
16_3023	Idaho	Payette	RPA- Interstate	Interstate	84	West	15.08	500	10
18_3002	Indiana	Benton	RPA- Other	U.S. Highway	41	South	—	500	8
18_3003	Indiana	Marshall	RPA- Other	U.S. Highway	31	North	—	500	1
18_3031	Indiana	Posey	Rural Minor Arterial	State Highway	62	West	—	500	7
19_3006	Iowa	Clinton	RPA- Other	U.S. Highway	30	East	318.3	500	10
20_0200	Kansas	Dickinson	RPA- Interstate	Interstate	70	West	283	500	7
20_3015	Kansas	Fiffey	RPA- Other	U.S. Highway	50	East	65.73	500	1
21_3016	Kentucky	Bullitt	RPA- Interstate	Interstate	65	North	106.59	500	11
26_0200	Michigan	Monroe	RPA- Other	U.S. Highway	23	North	2.02	500	9
27_3003	Minnesota	Nicollet	RPA- Other	State	15	North	65.9	500	10
27_3013	Minnesota	Hennepin	UPA- Other	U.S. Highway	169	South	140.62	500	10
28_3018	Mississippi	Tishomingo	RPA- Other	U.S. Highway	72	West	—	500	10
28_3019	Mississippi	Tishomingo	RPA- Other	U.S. Highway	72	West	—	500	10
31_3018	Nebraska	Buffalo	RPA- Interstate	Interstate	80	West	274.5	500	5
32_3010	Nevada	Elko	RPA- Interstate	Interstate	80	West	348.56	500	8
32_3013	Nevada	Elko	RPA- Interstate	Interstate	80	West	400.98	500	8
32_7084	Nevada	Clark	RPA- Interstate	Interstate	15	North	20.87	500	2
37_0200	North Carolina	Davidson	RPA- Other	U.S. Highway	52	South	91.49	500	11
37_3008	North Carolina	Cleveland	UPA	U.S. Highway	74	East	22.93	500	6
37_3011	North Carolina	Nash	RPA- Interstate	Interstate	95	North	129	500	9
37_3044	North Carolina	Durham	RPA- Interstate	Interstate	85	South	181.6	500	8
37_3807	North Carolina	Davidson	RPA- Other	U.S. Highway	52	North	22.98	500	8
37_3816	North Carolina	Durham	RPA- Other	State Highway	147	North	5.95	500	4
39_3013	Ohio	Brown	Rural Minor Arterial	U.S. Highway	68	South	21.7	500	3
39_3801	Ohio	Belmont	UPA - Other	U.S. Highway	7	South	12.33	500	6
4_0200	Arizona	Maricopa	RPA- Interstate	Interstate	10	East	109	500	9
4_7614	Arizona	Maricopa	RPA- Interstate	Interstate	10	West	130.5	500	5
40_3018	Oklahoma	Oklahoma	UPA- Interstate	Interstate	240	West	—	500	6
40_4160	Oklahoma	Pontotoc	UPA- Other	State Highway	3W	West	—	500	6
40_4162	Oklahoma	Comanche	RPA- Other	U.S. Highway	62	East	—	500	6
46_3012	South Dakota	Meade	RPA- Interstate	Interstate	90	East	37.98	500	9
5_3011	Arkansas	White	RPA- Other	U.S. Highway	67	South	11	500	5
53_0200	Washington	Adams	UPA- Other	State Highway	395	North	91.57	500	9
53_3011	Washington	Whatcom	UPA- Interstate	Interstate	5	South	259.7	500	5

Table 5. Summary of general information and site/project identification information for the projects used in New J and calibration (obtained from LTPP GPS-3 and SPS-2 and FHWA RPPR).

SHRP_ID	State	County	Functional Class	Route Signing	Route No.	Direction of Travel	Mile Point	Section Length, ft	Const. Month
53_3013	Washington	Spokane	RPA- Other	U.S. Highway	195	North	91.6	500	10
53_3014	Washington	Franklin	RPA- Other	U.S. Highway	395	North	26.11	500	4
53_3019	Washington	Benton	UPA- Interstate	Interstate	82	East	115.01	500	4
53_3813	Washington	Clark	UPA- Other	State	14	West	11.03	500	8
53_7409	Washington	Yakima	RPA- Interstate	Interstate	82	East	49	500	5
55_3008	Wisconsin	Ozaukee	RPA- Interstate	Interstate	43	North	26.54	500	12
55_3009	Wisconsin	Sheboygan	RPA- Other	State	23	East	258.94	500	10
55_3010	Wisconsin	Sheboygan	RPA- Other	State	23	West	262.23	500	10
55_3016	Wisconsin	Waushara	RPA- Other	U.S. Highway	51	North	122.32	500	6
55_6351	Wisconsin	Iowa	RPA- Other	U.S. Highway	18	East	—	500	6
55_6352	Wisconsin	Iowa	RPA- Other	U.S. Highway	18	East	—	500	6
55_6353	Wisconsin	Iowa	RPA- Other	U.S. Highway	18	East	—	500	6
55_6354	Wisconsin	Iowa	RPA- Other	U.S. Highway	18	East	—	500	6
55_6355	Wisconsin	Dane	RPA- Other	U.S. Highway	18	East	—	500	6
6_3005	California	Siskiyou	RPA- Interstate	Interstate	5	North	14.58	500	11
6_3021	California	San Diego	RPA- Interstate	Interstate	8	East	55.1	500	4
6_3030	California	Shasta	RPA- Interstate	Interstate	5	South	43.18	500	10
6_3042	California	San Joaquin	RPA- Interstate	Interstate	5	South	48.6	500	6
8_0200	Colorado	Adams	RPA- Interstate	Interstate	76	East	18.46	500	10
8_3032	Colorado	Garfield	RPA- Interstate	Interstate	70	East	95.75	500	6
GA1	Georgia	Newnan	—	Interstate	85	South	6335	—	7
GA2	Georgia	La Grange	—	Interstate	85	South	4949	—	7
MI1	Michigan	Clare	—	US Highway	10	East/West	3616	—	7
MN7	Minnesota	Roseville	—	State Highway	36	East/West	7377	—	7
NC1	North Carolina	Rocky Mount	—	Interstate	95	North /South	7395	—	7
NC2	North Carolina	Greensboro	—	Interstate	85	North	3630	—	7
NY1	New York	Catskill	—	Route	23	West	4025	—	7
NY2	New York	Otego	—	Interstate	88	West	7195	—	7
WI4	Wisconsin	Waukesha County	—	State Highway	164	South	8937	—	7
WI5	Wisconsin	Kenosha County	—	State Highway	50	East	1205	—	7
WI6	Wisconsin	Brown County	—	State Highway	29	East	3269	—	7
WI7	Wisconsin	Iowa County	—	US Highway	18/151	East	2173	—	7
WV1	West Virginia	Charleston	—	Interstate	77	North /South	1570	—	7

*UPA = Urban Principal Arterial; RPA = Rural Principal Arterial.

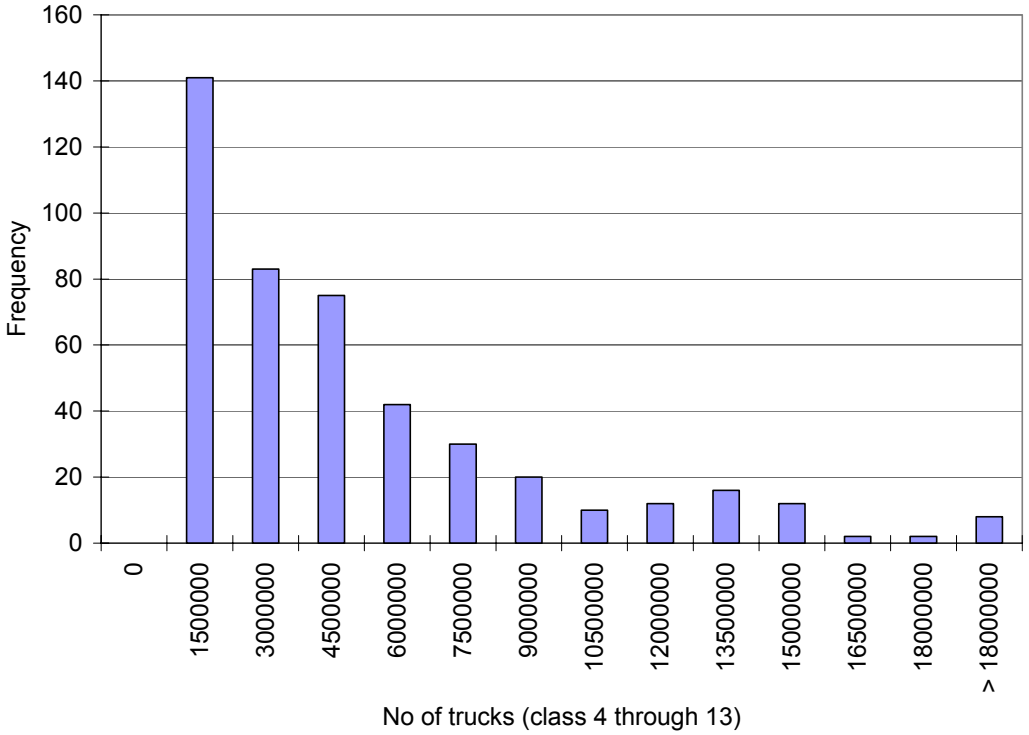

Figure 14. Frequency of number of trucks over analysis period for JPCP calibration sections.

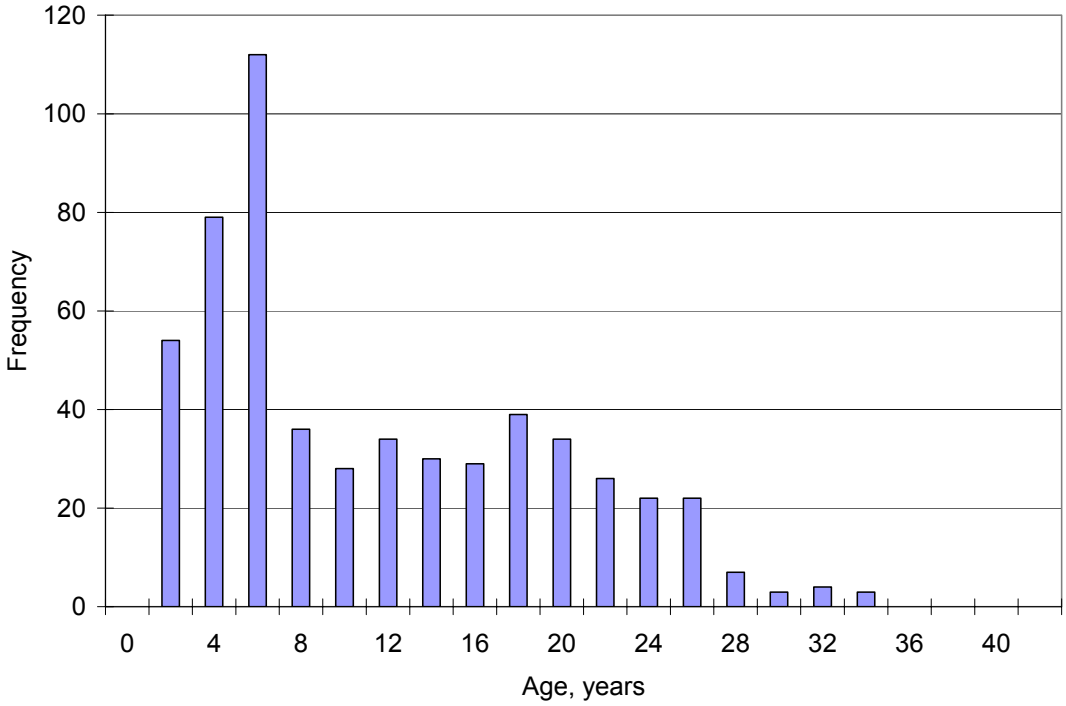

Figure 15. Frequency of age of JPCP sections used in calibration.

Field Calibration of Transverse Cracking

The fatigue cracking damage algorithm was run for each JPCP calibration section over its life where cracking data were available. A plot of Minor's damage versus observed percent slabs cracked was prepared and examined. A best fit s-shaped curve was fit to the data. Obvious outliers were examined to see if any erroneous input data existed and quite often this was the case. The damage algorithm was often changed over a period of about two years and this required a rerun of the software for each section (over a week of work for each recalibration). This process was repeated many times as the fatigue damage algorithm evolved over time.

This calibration procedure relates the theoretical damage number with actual observed field slab cracking. If there is a strong positive relationship between these the damage value and the percent cracked slabs then the fatigue cracking model algorithm could be used to predict cracking for a given JPCP design located in a given climate on a given subgrade and subjected to a given traffic loading. The final "nationally calibrated" cracking model is shown in figure 16. This plot shows a fairly good positive relationship between the calculated fatigue damage and field cracking for nearly 200 JPCP sections located throughout the U.S. with 516 observations (most sections had time series data). The data and best fit curve follows a typical s-shaped curve similar to the several calibration curves developed over the past 30 years with smaller amounts of data and less sophisticated damage algorithms.

The final calibration model which shows percentage of slabs with transverse cracks of all severities in a given traffic lane is used as the measure of transverse cracking and is predicted using the following model for both bottom-up and top-down cracking:

$$CRK = \frac{1}{1 + FD^{-1.68}} \tag{3.4.2}$$

where,

CRK = predicted amount of bottom-up or top-down cracking (fraction).
FD = fatigue damage calculated using the equation 7 algorithm.

Model Statistics:
R^2 = 0.75
N = 516 observations
SEE = 6.9 percent

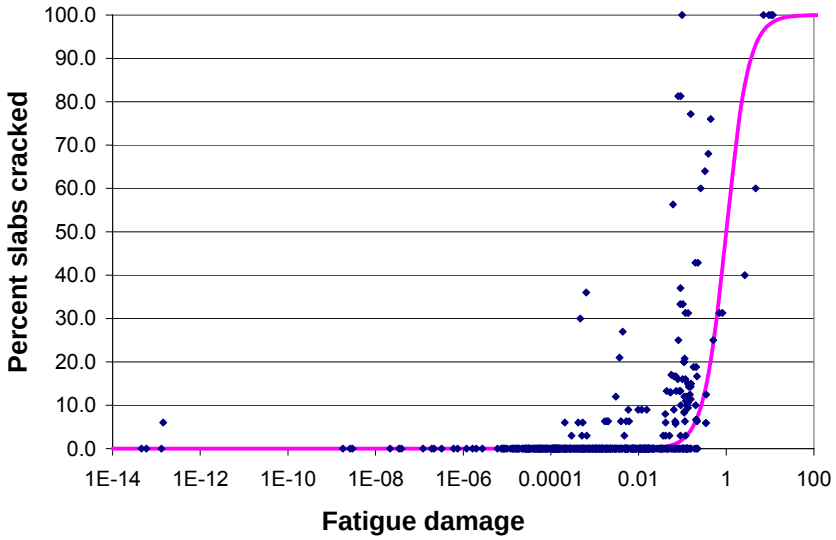

Figure 16. JPCP cracking model shown with the field data.

The R^2 and the standard error of the estimate (SEE) are reasonable considering the uncertainties and unknowns involved is such estimations. The residual error includes several components:

- Errors in the collection and storage of the observed field cracking data for each JPCP section (e.g., two survey crews would report different results for the same section, also LTPP and other sections are very short such as 500 ft and may not well represent a longer project length).
- Errors in the estimation of each input for the JPCP sections included (e.g., traffic loadings, material properties, layer thicknesses, bonding of layers and lane/shoulder LTE). There was a significant amount of missing data in the LTPP database and some of these were estimated to avoid loosing more sections for the calibration.
- Limitations or errors involved in the fatigue damage algorithm itself (e.g., accuracy of critical stress calculation, Minor's damage model has many limitations).
- Random unexplained residual (or pure) error of fatigue fracture (e.g., differences that would exist even between pairs of identical JPCP sections).

Any comparison of model predicted distress and observed field measurements of distress should be examined in light of all of these residual errors and variabilities. However, this comparison is an essential step in model validation as this gives an indication of the ability of the JPCP slab cracking model to accurately predict cracking for JPCP. The predictive capability and accuracy of the distress models were evaluated using statistical analysis as follows:

1. Determine the correlation between predicted and measured distress (R^2). The 0.75 value indicates that the model explains 75 percent of the total variability in cracking for the 516 JPCP observations throughout the U.S.

2. Determine the standard error of the estimate between predicted and observed cracking (SEE). This value is 6.9 percent includes all of the sources of error listed above.
3. Use paired t-test analysis to determine whether there is a significant difference (or bias) on average between observed and predicted cracking for the in-service calibration JPCP analyzed.

Figure 17 was prepared which shows the same data presented in figure 16, only now the predicted cracking is plotted versus the observed slab cracking for all the sections. The scatter about the one-to-one line is an indication of the residual error involved in crack prediction plus any error in the measurement of the observed cracking. If there are more data points above or below the line this might indicate a bias in prediction. The paired t-test will resolve this issue. Figure 18 shows the residual (observed – predicted cracking) plotted against the predicted cracking. The horizontal band of data indicates no abnormality or trend.

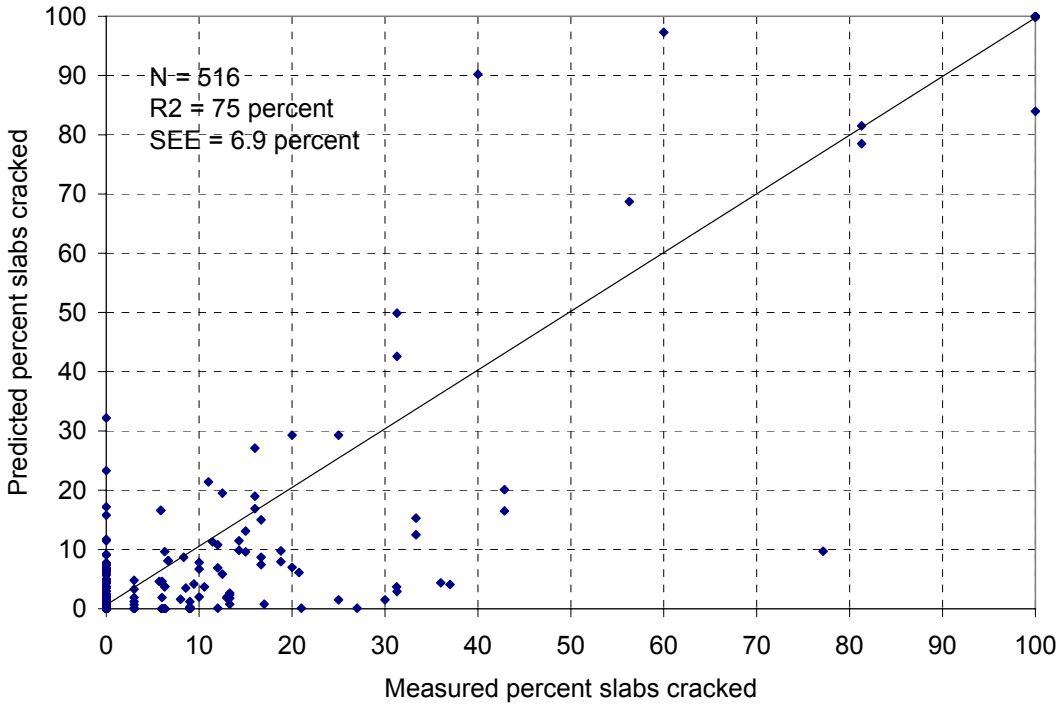

Figure 17. Predicted versus observed transverse cracking for JPCP calibration sections.

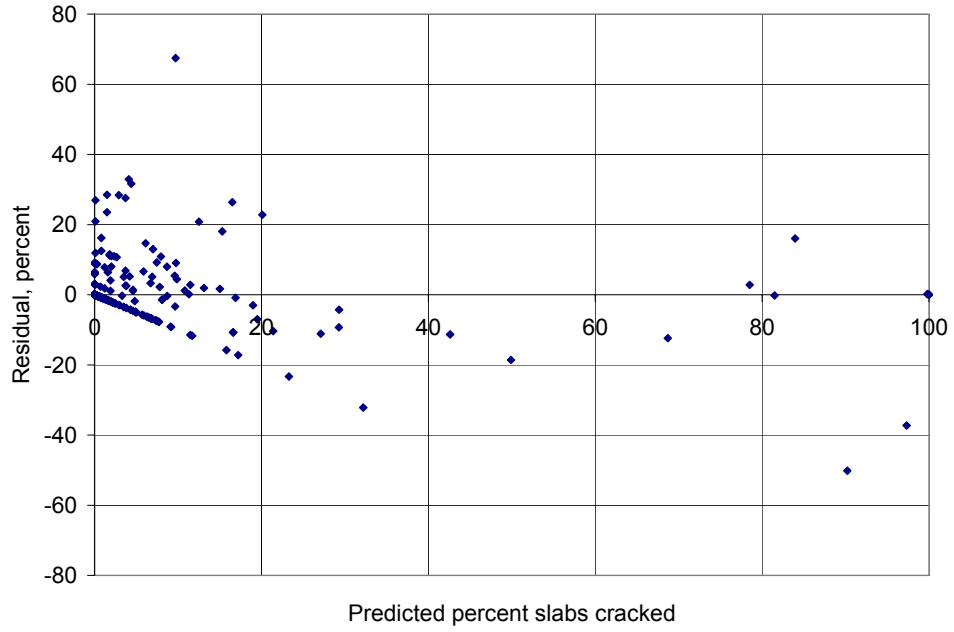

Figure 18. Residual (predicted – observed) versus predicted percent slabs cracked for JPCP calibration sections.

The results presented in figures 17 and 18 shows that there was reasonable correlation between the predicted and measured distress (R^2 = 75 percent) with reasonable levels of error (standard error of residual = 6.9 percent) between observed and predicted slab cracking. The plot of predicted cracking versus residuals also showed no appreciable trends implying that the data used in analysis was independent.

A paired t-test comparison was made to test the null hypothesis that the predicted and observed cracking are on the average the same number. This test would show if there was any bias (over or under predicting on average) between the observed and predicted cracking. The analysis and results are shown in table 6 and indicate that there is no evidence on which to reject the null hypothesis (e.g., using a two tailed test at say a 5 percent level of significance). In other words, the results confirm the expectation that the model does not consistently over or under predict transverse cracking for the calibration data.

Table 6. Results of paired t-test analysis of observed and predicted transverse cracking of JPCP calibration sections.

t-Test: Paired Two Sample for Means

	Observed	Predicted
	Variable 1	*Variable 2*
Mean (percent cracked slabs)	4.064990564	3.634961
Variance	181.8583504	176.4344
Observations	516	516
Pearson Correlation	0.86549177	
Hypothesized Mean Difference	0	
Df	515	
t Stat	1.406596131	
P(T<=t) one-tail	0.080075156	
t Critical one-tail	1.647817953	
P(T<=t) two-tail	0.160150312	
t Critical two-tail	1.964581315	

Given these results it is recommended that this model can be used to predict cracking of JPCP as a function of Minor's fatigue damage with reasonable accuracy over a large set of design, traffic, and climatic conditions.

Figure 19 shows an example of predicted cracking versus age for a given JPCP. Predictions at the 50 percent level and at a higher level of reliability are provided which will be explained in a later section. Note that this prediction is valid only when the fatigue damage is calculated according to the procedure described in this section. If the fatigue damage algorithm is changed or if improper inputs are used the model may not predict well.

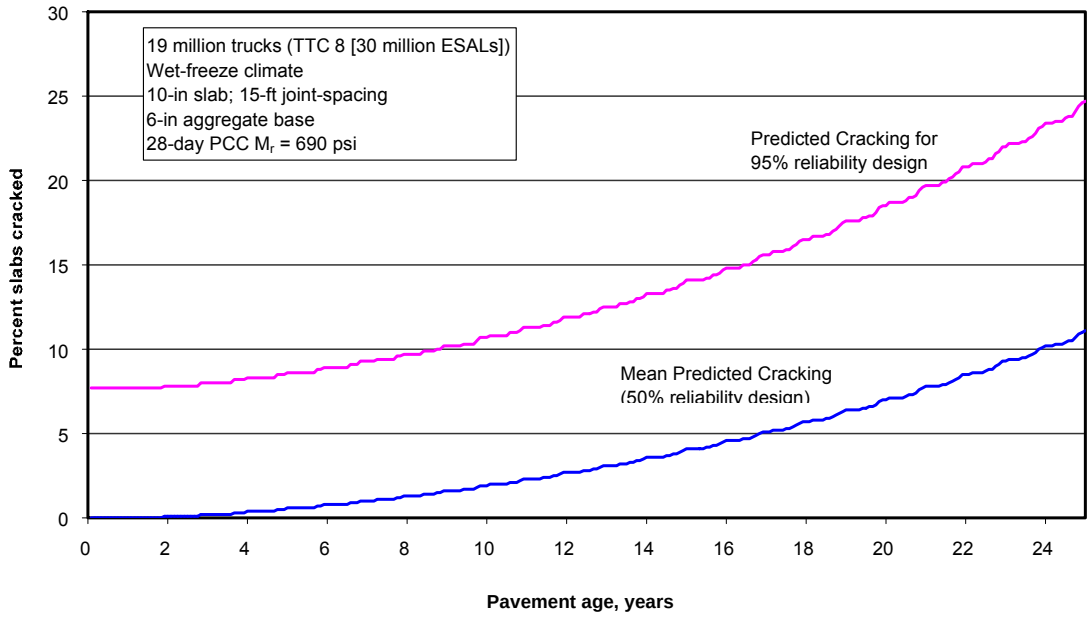

Figure 19. Example JPCP cracking predictions given by the cracking model.

Top-Down and Bottom-Up Cracking Combined

For JPCP transverse cracking, both bottom-up and top-down modes of cracking are considered. Under typical service conditions, the potential for either mode of cracking is present in all slabs. Any given slab may crack either from bottom-up or top-down, but not both. Therefore, the predicted bottom-up and top-down cracking are not particularly meaningful by themselves, and combined cracking must be determined, excluding the possibility of both modes of cracking occurring on the same slab.

The total amount of cracking is determined as follows:

$$TCRACK = \left(CRK_{Bottom-up} + CRK_{Top-down} - CRK_{Bottom-up} \cdot CRK_{Top-down}\right) \cdot 100\% \qquad (13)$$

where,

$TCRACK$ = total cracking (percent).
$CRK_{Bottop\text{-}up}$ = predicted amount of bottom-up cracking (fraction).
$CRK_{Top\text{-}down}$ = predicted amount of top-down cracking (fraction).

Equation 13 assumes that a slab may crack from either bottom-up or top-down, but not both.

Range of the JPCP Calibration Data for Slab Transverse Cracking

A summary table was prepared to show the mean and the minimum and maximum of each of the key design inputs. Table 7 shows these results and indicates the following facts about the calibration database for JPCP.

- Slab thickness ranged from 6 to 13-in with a mean of 9.5-in.
- Base type included unbound aggregates, asphalt stabilized, and cement stabilized.
- Joint spacing ranged from 11 to 30-ft with an average of 17-ft.
- Joint load transfer consisted of 56 sections with no dowels and 124 with dowels. The bar diameters ranged from 1.00-in to 1.50-in.
- Approximately 28 percent of the sections had a widened slab (2-ft typical).

Table 7. Summary of the mean and range of key inputs used in the calibration procedure for slab cracking.

Pavement Design Feature	Statistics
PCC thickness, in	• Mean = 9.53 • Maximum = 13.3 • Minimum = 6.4
Base type (used in pavement sections)	• Dense HMA/asphalt treated material = 29 • Cement stabilized (dense) = 20 • Crushed stone/gravel (dense) = 55 • Lean concrete = 29 • Open Graded Asphalt Concrete = 26 • Soil cement = 8
Joint spacing, ft	• Mean = 16.9 • Maximum = 30.0 • Minimum = 11.5
Load transfer	No dowel = 56 sections 1-in dowel = 9 1.125-in dowel = 9 1.25-in dowel = 48 1.375-in dowel = 3 1.5-in dowel = 55
Tied PCC shoulder	Yes = 130 No = 50
Lane width	12-ft = 130 14-ft = 50
Random joint spacing	Yes = 40 No = 140

6.0 SENSITIVITY OF DESIGN FACTORS

Another important aspect of validation of the new cracking model is sensitivity analysis. A detailed sensitivity analysis was conducted to determine how all of the inputs to the model would affect cracking of JPCP. All of these results showed that the direction of effect was consistence with engineering mechanics and field experience. This section illustrates the sensitivity of a few of the key inputs on the cracking output.

JPCP Design Features

Joint Spacing and Slab Thickness

The joint spacing is a critical JPCP design factor that affects structural and functional performance of JPCP, as well as construction and maintenance cost. The critical stresses in JPCP increase rapidly with increasing joint spacing. Joint spacing must be selected within the context of design features such as slab thickness, slab width, PCC materials properties, base type, and subgrade stiffness to balance performance and cost. A particular joint spacing may be adequate for a given set of design features, but inadequate for another. The interaction between slab thickness and joint spacing is shown in figure 20. As joint spacing increases the percent slabs cracked also increases in an s-shaped curve, similar to the C-factor in Westergaards stress equation. In general, thicker slabs can have longer joint spacing resulting in cost optimization.

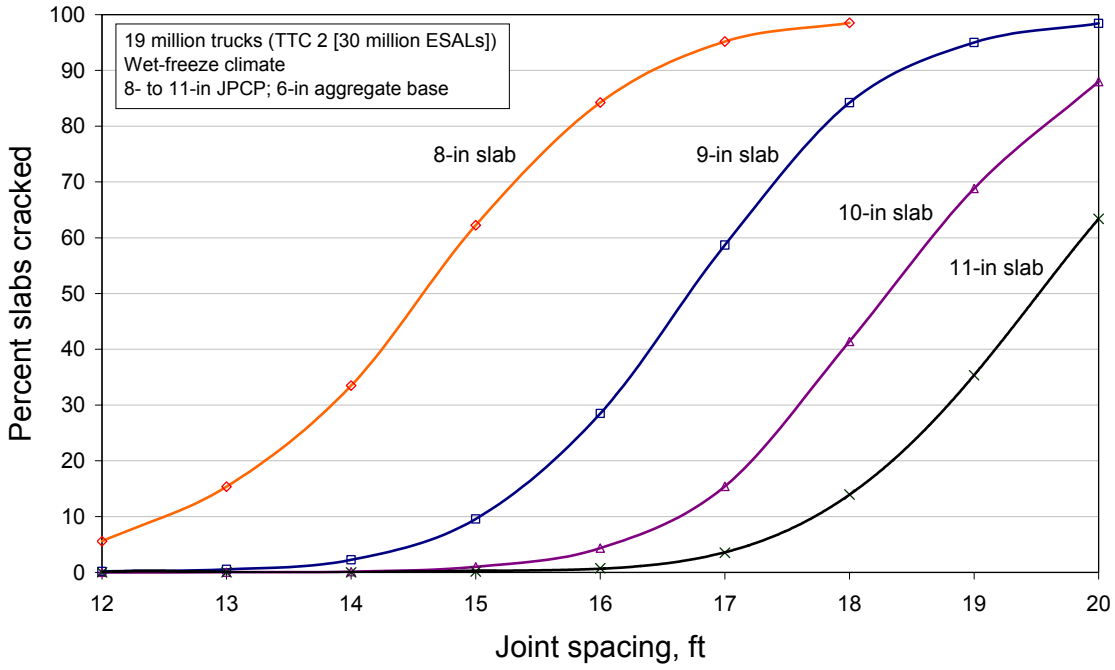

Figure 20. Sensitivity of JPCP transverse cracking to slab thickness and joint spacing.

In general, a short joint spacing (e.g., 15 ft) is recommended; however, there is no need to make joint spacing less than 12 ft, since the lane width is 12 ft. If random joint spacing is used, the long and short panels should be evaluated separately. For example, if 12-13-19-18 ft joint

spacing pattern is used, the 12- and 13-ft panels should grouped and analyzed using 13 ft joint spacing, and the 18- and 19-ft panels should be grouped and analyzed using 19 ft joint spacing. The average cracking from the two designs is the expected cracking in the random jointed section since they both represent 50 percent of the number of total slabs.

Edge Support

Tied PCC shoulders and widened slabs can significantly improve JPCP cracking by reducing critical stresses. The shoulder type also affects the amount of moisture infiltration into the pavement structure. The effects of moisture infiltration are considered in the determination of seasonal moduli values of unbound layers. The structural effects of the edge support features are directly considered in the design process, as illustrated in figure 21 for cracking. The inputs for these design features used in calibration are as follows:

Tied PCC Shoulder – for tied concrete shoulders the long-term LTE between the lane and shoulder must to be provided. The LTE is defined as the ratio of deflections of the unloaded and loaded slabs. The higher the LTE, the greater the support provided by the shoulder to reduce critical responses of the mainline slabs. Typical long-term deflection LTE are:

- 50 to 70 percent for monolithically constructed tied PCC shoulder.
- 30 to 50 percent for separately constructed tied PCC shoulder.
- Untied concrete shoulders or other shoulder types do not provide significant support; therefore, a low LTE value should be used (e.g., 10 percent due to the support from extended base course).

Widened Slab – widened slabs improve JPCP performance by effectively moving the mean wheelpath well away from the pavement edges where the critical loadings occur. The design input for widened slab is the slab width. The critical point for fatigue damage shifts to the lane to lane longitudinal joint when a widened slab is used. This joint was assumed to have 70 percent long term load transfer efficiency (LTE). Cracks will initiate from this joint, not the traditional lane to outside shoulder joint due to strong impact of the widening.

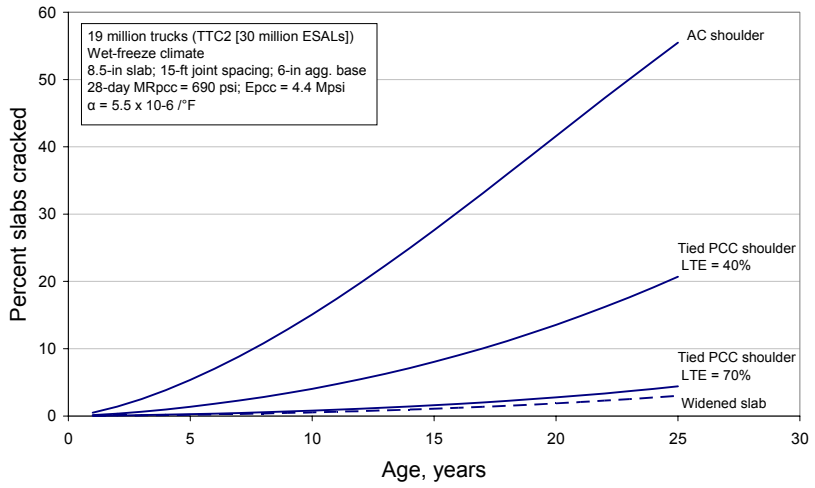

Figure 21. Effects of edge support on JPCP transverse cracking.

Concrete Strength and Modulus of Elasticity

Both the modulus of rupture (MR) and the modulus of elasticity (E_c) have an effect on slab cracking. The MR affects the ratio of stress to strength in Miner's damage model. The E_c effects the stress calculated in the slab. The higher the E_c the higher the calculated stress, and thus the higher the fatigue damage. However, there is typically a strong correlation between MR and E_c for a given concrete mixture. Therefore, the sensitivity analysis must vary both of these inputs in a rational way to show their true impact.

This was accomplished as shown in figure 22 where the MR is varied but the E_c / MR ratio is held constant as it would typically be for a given concrete mixture. The plot shows that increased MR still has a very significant effect on reducing the JPCP slab cracking due to reduced fatigue damage. This may have some limitations in that very high strength mixes may have higher shrinkage characteristics that would increase the upward curling of the slabs increasing the potential for top down cracking. Since shrinkage is a direct input to the fatigue damage model, if the extent of increased shrinkage were known, the impact could be determined.

It is noted here that the design input MR is the 28-day mean third point loading value. This value is normally much higher than that specified in the construction specifications. Thus, the mean MR must be input, not the lower construction specification value.

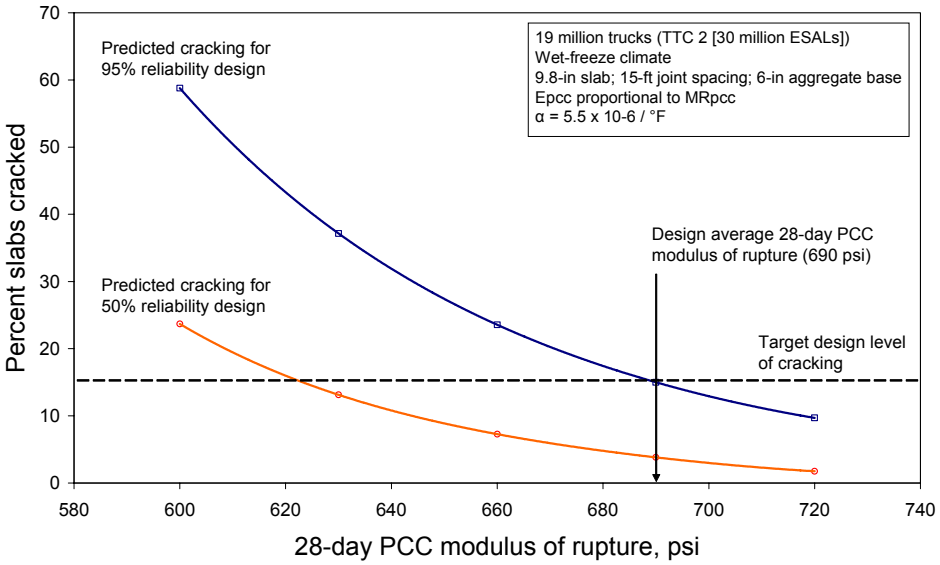

Figure 22. Sensitivity of JPCP transverse cracking to PCC strength, holding the ratio of PCC elastic modulus to PCC strength constant.

Base Type

One of the most challenging aspects of concrete pavement design is choosing a base type and the specification of its properties. Field studies have shown that the base characteristics can make or break a concrete pavement. This is particularly true for non doweled JPCP where the corner deflections under load are much higher than a doweled JPCP. High differential deflections lead to erosion, joint faulting, and loss of support and eventually slab cracking.

Figure 23 was prepared to illustrate the impact of base type on cracking of JPCP. The same heavily trafficked pavement was placed on three base types: unbound aggregate (6-in), cement treated (4-in), and asphalt treated (4-in). The unbound aggregate base shows more cracking than the treated bases. The treated bases were assumed to be bonded to the slab for the first 5-years of the pavements 20 year life. This is primarily due to the higher modulus of elasticity of the treated base courses which tend to reduce the critical stress in the slabs under loadings. Of course, each of the treated bases could be modified to have higher or lower long term moduli and the results would slightly change. The fatigue cracking model does not have the ability to show the effect of erosion on the modulus of the base course nor does it have the ability to show loss of support along the edge due to erosion of the base. It does include upward curling due to temperature and moisture gradient which would show some loss of support.

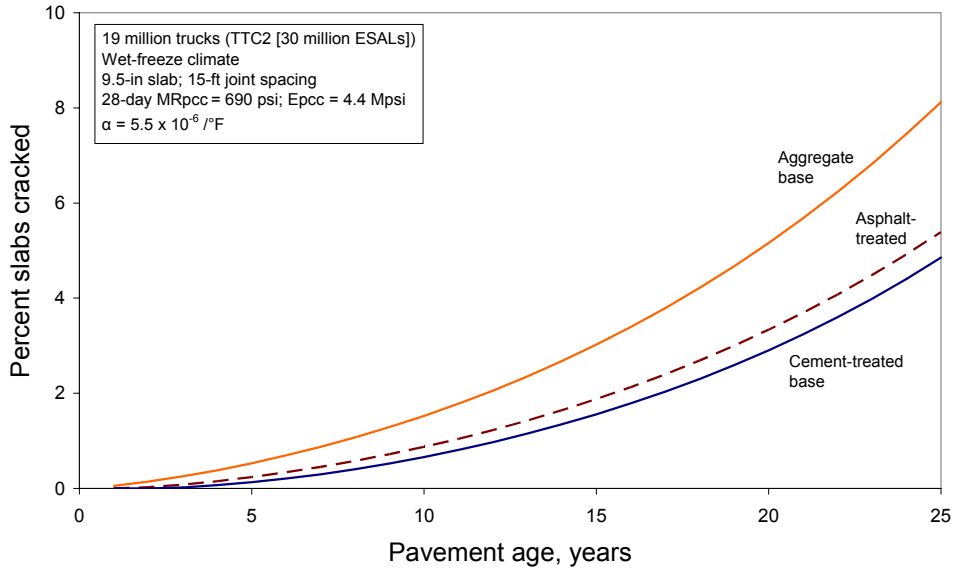

Figure 23. Effect of base type on JPCP slab cracking.

Concrete Thermal Coefficient of Expansion

The thermal coefficient of expansion of the concrete used in the JPCP directly effects the thermal curling stress in the slab. A higher coefficient would result in higher critical stresses and increased fatigue damage in the slab. Figure 24 shows a plot of a range of thermal coefficients from relatively low to high as might exist within a given State highway agency. The coefficient depends greatly on the main aggregate source used in the mix which ranges from 3.5 to 8.0 * 10^{-6}

per degree F. Figure 24 shows that the thermal coefficient of expansion has a very great effect on transverse cracking of JPCP. This input has never before been used in the design of JPCP and probably explains why some pavements had much more cracking than others with the same design.

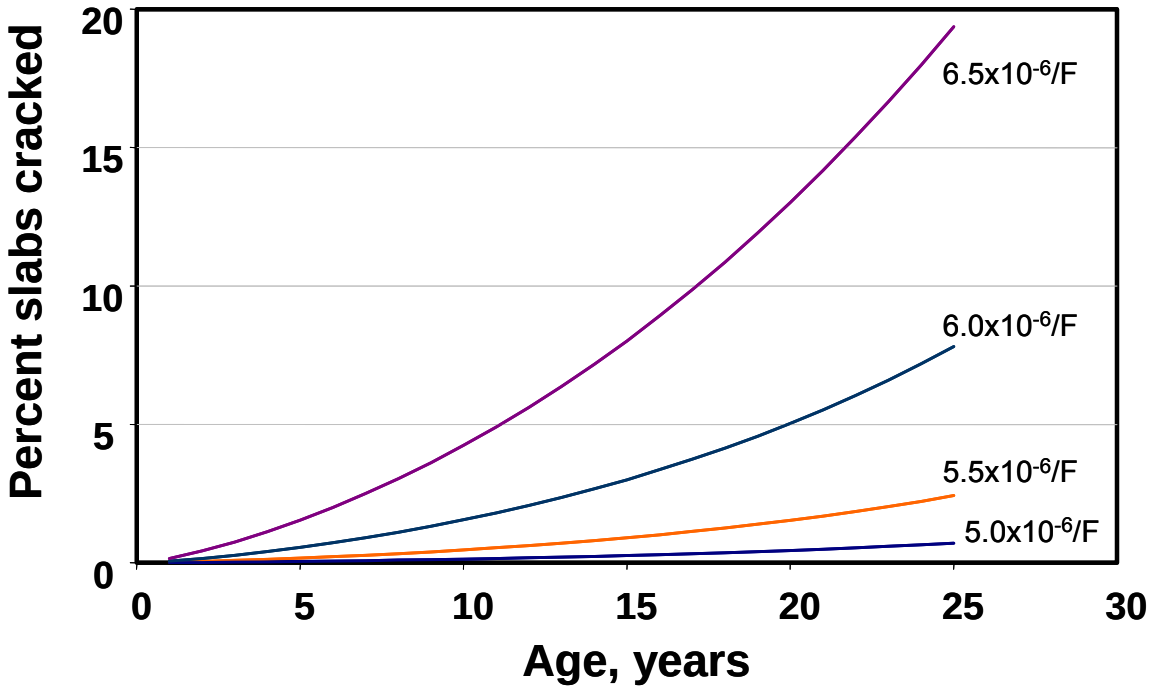

Figure 24. Effect of the thermal coefficient of expansion of concrete on JPCP slab cracking.

Climate/Geographical Regions

The United States is a very large country geographically and includes a very wide range of climates in which pavements must perform. It is expected that climate has a very significant effect on performance but this has been difficult to demonstrate because prediction models have not been available that show this effect. Figure 25 was prepared using identical JPCP designs and subgrade supports for four climates: Illinois (wet-freeze), Florida (wet-nonfreeze), North Dakota (dry-freeze), and Arizona (dry-nonfreeze). The nonfreeze areas have far more solar radiation due to less cloud cover (and also perhaps a wider change in temperatures from day to night) and thus the thermal curling is apparently greater resulting in increased transverse cracking in these climates (assuming the same identical designs). This result is extremely interesting in that it clearly shows that you cannot adopt a design that works well in one climate and build it in another and hope for the same performance.

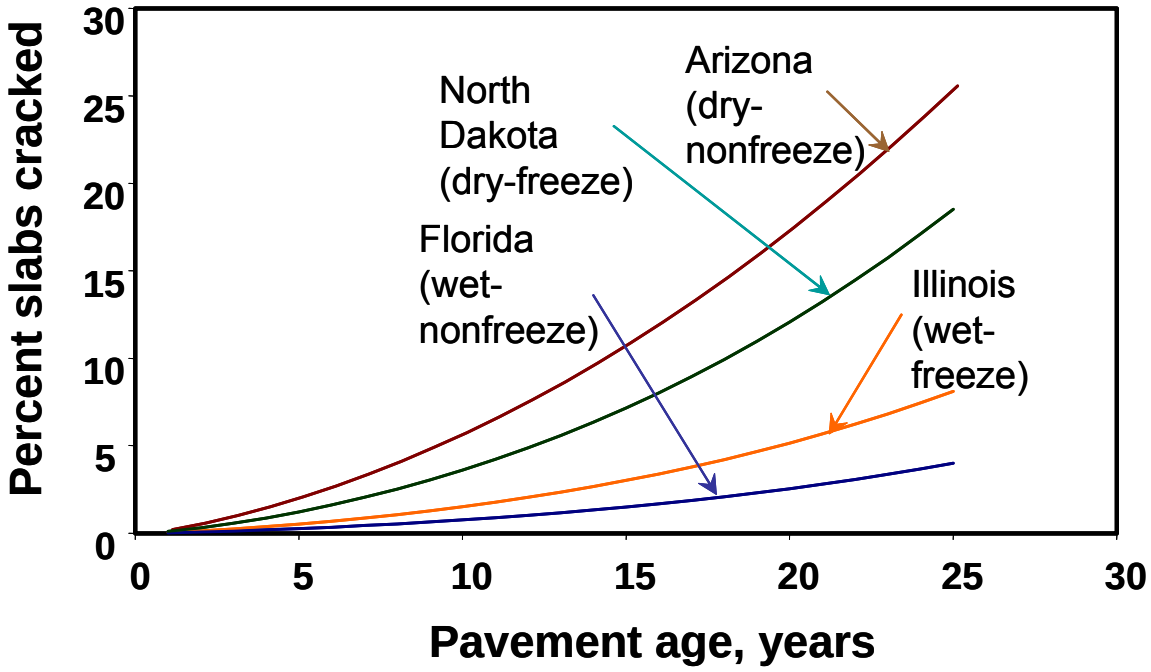

Figure 25. Effect of climate on JPCP slab cracking (note all sections have similar designs and subgrade support).

7.0 DESIGN RELIABILITY

A more detailed account of JPCP cracking reliability is given in Appendix BB and a summary is provided here because it is critical to model calibration. A large amount of uncertainty and variability exists in pavement design and construction, as well as in the application of traffic loads and climatic factors over the design life. In the mechanistic-empirical design, the key outputs of interest are the individual distress quantities (e.g., faulting, transverse cracking, and smoothness for JPCP). Therefore, the predicted distress is the random variable of interest in reliability design. Quantification of the distribution this variable assumes for all possible estimates of the mean and its associated moments is of interest for reliability estimation. In this Guide, the variability associated with the predicted distress quantity is estimated based on calibration results, after a careful analysis of the differences between the predicted versus actual distresses in the field. For design purposes, the design reliability is established based on knowledge of variation of a given performance around the mean prediction.

Design reliability for the individual pavement distress models (i.e., cracking, faulting, and CRCP punchouts) are based on the standard error of the estimates of each individual model obtained through the calibration process. These estimates of error include a combined input variability, variability in the construction process, and model or pure error. The larger this residual error the more impact reliability has on the design.

The desired level of reliability is specified along with the acceptable level of distress at the end of design life in defining the performance requirements for a pavement design in this Guide. For example, one criterion might be to limit percent slabs cracked to 8 percent at a design reliability of 90 percent. Thus, if a designer designed 100 projects, 90 of these projects would exhibit slab cracking less than 8 percent at the end of the design life. Of course, the higher the design reliability for a given distress, the higher the initial cost of the pavement; however, the future maintenance cost would be lower for the higher-reliability design.

Cracking Reliability

The reliability design is obtained by determining the predicted cracking at the desired level of reliability as follows:

$$CRACK\_P = CRACK + STD_{CR} \bullet Z_P \qquad (14)$$

$$CRACK\_P \leq 100\ \%$$

where,

$CRACK\_P$ = predicted cracking at the reliability level P, percent of slabs.
$CRACK$ = predicted cracking based on mean inputs (corresponding to 50% reliability), percent of slabs.
STD_{CR} = standard deviation of cracking at the predicted level of mean cracking:

$$STD_{CR} = -0.00172\ CRACK^2 + 0.3447\ CRACK + 4.6772 \qquad (15)$$

Z_P = standard normal deviate (one-tailed distribution).

For example, if the predicted cracking based on mean inputs is 10 percent, the predicted cracking for 90 percent reliability design is obtained as follows:

$$
\begin{aligned}
STD_{CR} &= -0.00172 \bullet 10^2 + 0.3447 \bullet 10 + 4.6772 \\
&= 8.0\ \% \\
Z_P &= 1.28 \\
CRACK\_P &= 10 + 8.0 \bullet 1.28 \\
&= 20.2\ \%
\end{aligned}
$$

Thus, if the design criteria are less than 10 percent slab cracking at 90 percent reliability, the structural capacity must be increased until *CRACK_P* is less than 10 percent. Equation 15 may be modified based on local calibration.

Figure 19 showed an example of predicted cracking over the design life based on mean input (50% reliability) and that for 95 percent reliability design. Figure 26 shows the required slab thickness at different levels of reliability of an example design. The reliability level corresponding to different slab thicknesses can also be obtained from this figure.

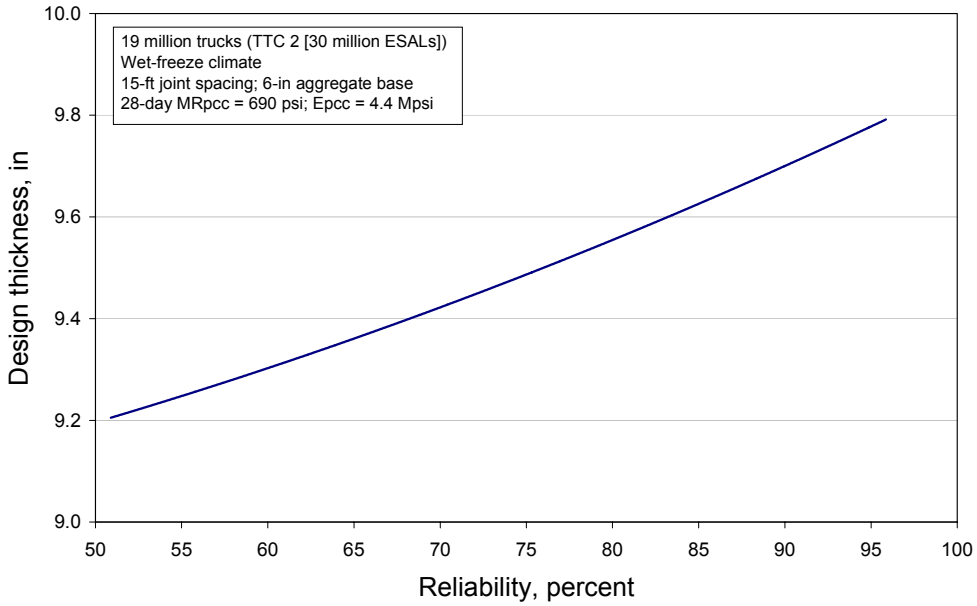

Figure 26. Required slab thickness at different reliability level for an example design.

REFERENCES

1. Khazanovich, L., H. T. Yu, S. Rao, K. Galasova, E. Shats, and R. Jones. (2000). *ISLAB2000 - Finite Element Analysis Program for Rigid and Composite Pavements*. User's Guide. ERES Consultants Division of Applied Research Associates, Inc., Champaign, IL.
2. Yu, H. T., K. D. Smith, M. I. Darter, J. Jiang and L. Khazanovich (1998). *Performance of Concrete Pavements Volume III - Improving Concrete Pavement Performance*. Final Report, FHWA-RD-95-111, Federal Highway Administration, McLean, VA.
3. Poblete, M. (1986). *Informe Anual 1986*, Control y Seguimiento de Pavimentos de Hormigon, IDIEM-Direccion de Vialidad, Universidad de Chile.
4. Darter, M. I., J. M. Beck, M. B. Snyder, and R. E. Smith (1985). *Portland Cement Concrete Pavement Evaluation System-COPES*, NCHRP Report 277, Transportation Research Board, Washington, D.C.
5. Khazanovich, L., M. Darter, R. Bartlett, and T. McPeak (1998). *Common Characteristics of Good and Poorly Performing PCC Pavements*. Report FHWA-RD-97-131. Federal Highway Administration, Washington, D.C.
6. Mindess, S., and J. F. Young (1981). *Concrete*. Prentice-Hall, Englewood Cliffs, NJ.
7. Janssen, D. J. (1987). "Moisture in Portland Cement Concrete," *Transportation Research Record 1121*. Transportation Research Board, Washington, D.C.
8. Rao, C., E. J. Barenberg, M. B. Snyder, and S. Schmidt (2001). "Effects of Temperature and Moisture on the Response of Jointed Concrete Pavements." *Proceedings*, *7th International Conference on Concrete Pavements*, Orlando, Florida.
9. Springenschmid, R. and W. Fleischer (2001). "Recent Developments in the Design and Construction of Concrete Pavements for German Expressways," *Proceedings*, *7th International Conference on Concrete Pavements*, Orlando, Florida.
10. Springenschmid, R., and E. Hiller (September 1998). "Influence of Temperature During Curing on Stresses in Concrete Pavements," *Proceedings, 8th International Symposium on Concrete Roads*, Theme II, Lisbon, Portugal.
11. Springenschmid, R. and M. Mangold (1994). "Curing of Concrete Pavements to Control Thermal Stresses," *Proceedings, 7th International Symposium on Concrete Roads*, Vienna, Austria.
12. Hall, K. T., M .I. Darter, T. E. Hoerner, and L. Khazanovich (1997). *LTPP Data Analysis—Phase I: Validation of Guidelines for k-Value Selection and Concrete Pavement Performance Prediction*. Technical Report FHWA-RD-96-198, Federal Highway Administration, McLean, VA.
13. Owusu-Antwi, E. B., L. Titus-Glover, L. Khazanovich, and J. R. Roesler. (1997). *Development and Calibration of Mechanistic-Empirical Distress Models for Cost Allocation*. Final Report, Federal Highway Administration, Washington, D.C.
14. McGhee, K.H. (1995). *Design, Construction, and Maintenance of PCC Pavement Joints*. Synthesis of Highway Practice 211. Transportation Research Board, National Research Council, Washington, DC.
15. Christory, J. P. (1990). "Assessment of PIARC Recommendations on the Combating of Pumping in Concrete Pavements." *Sixth International Symposium on Concrete Roads*. Madrid, Spain, 1990.
16. Permanent International Association of Road Congresses (1987). *Combating Concrete Pavement Slab Pumping by Interface Drainage and Use of Low-Erodability Materials: State*

of the Art and Recommendations, Permanent International Association of Road Congresses, Paris, France.
17. Darter, M. I. (1992). *Report on the 1992 U.S. Tour of European Concrete Highways*, Report FHWA-SA-93-012, Federal Highway Administration, Washington, D.C.
18. Larson, R.M., S. Vanikar, and S. Forster (date). *Summary Report—U.S. Tour of European Highways (U.S. Tech)—Follow-up Tour of Germany and Austria*. Report FHWA-SA-93-080. Federal Highway Administration, Washington, D.C.
19. Darter, M. I., H. L. Von Quintus, Y. J. Jiang, E. B. Owusu-Antwi, and B. M. Killingsworth (1997). *Catalog of Recommended Design Features* (CD-ROM). NCHRP Project 1-32. Transportation Research Board, National Research Council, Washington, D.C.
20. Chou, Y.T. (1981). *Structural Analysis Computer Programs for Rigid Multicomponent Pavement Structures with Discontinuities- WESLIQID and WESLAYER; Report 1: Program Development and Numerical Presentations; Report 2: Manual for the WESLIQID Finite Element Program; Report 3: Manual for the WESLAYER Finite Element Program*. Technical Report GL-81-6, U.S. Army Engineer Waterways Experiment Station, May.
21. ERES Consultants (1998). *Pavement SubsurfaceDrainage Design*. Reference Manual, NHI Course No. 13126. National Highway Institute, Washington, D.C.
22. Miner, M. A. (1945). "Cumulative Damage in Fatigue," *Transactions*, American Society of Mechanical Engineers, Vol. 67, pp. A159-A164.
23. Khazanovich, L. (1994). *Structural Analysis of Multi-Layered Concrete Pavement Systems*. Ph.D. Thesis, University of Illinois at Urbana-Champaign.
24. Hoerner, T. E, M. I. Darter, L. Khazanovich, L. Titus-Glover, and K. L. Smith (2000). *Improved Prediction Models for PCC Pavement Performance Specifications, Volume I: Final Report.* Report No. FHWA-RD-00-130, Federal Highway Administration, Washington, D.C.
25. Zollinger, D. G., N. Buch, D. Xin, and J. Soares (1999). *Performance of Continuously Reinforced Concrete Pavements: Volume VII: Summary*. Final Report, FHWA-RD-98-102, PCS/Law Engineering.
26. Gharaibeh, N. G., M. I. Darter, and L. B. Heckel (1999). "Field Performance of CRCP in Illinois," Report FHWA-IL-UI-268, Illinois Department of Transportation.
27. Simpson, A. L., Rauhut, J.B., Jordahl, P.R., Owusu-Antwi, E., Darter, M.I., Ahmad, R., Pendleton, O., Lee, Y-H., (1994). "Sensitivity Analysis for Selected Pavement Distresses," Report SHRP-P-393, Strategic Highway Research Program.
28. LaCourseiere, S. A., M. I. Darter, and S. A. Smiley (1978). *Structural Distress Mechanisms in Continuously Reinforced Concrete Pavement*, Transportation Engineering Series No, 20, University of Illinois at Urbana-Champaign.
29. Zollinger, D. G., and E. J. Barenberg (1990). *Continuously Reinforced Pavements: Punchouts and Other Distresses and Implications for Design*, Project IHR - 518, Illinois Cooperative Highway Research Program, University of Illinois at Urbana-Champaign.
30. Tang, T., D. G. Zollinger, and B. F. McCullough (1996). "Field Tests and Analyses of Concrete Pavement in Texarkana and La Porte, Texas," Research Report 1244-7, Texas Transportation Institute, Texas A&M University, College Station, TX.
31. Darter, M. I. (1988). "CRCP Distress Study on I-77 Fairfield and Chester Counties, South Carolina," ERES Consultants, Inc., Champaign, IL.

32. Selezneva O. I., D. Zollinger, and M. Darter (2001). "Mechanistic Analysis of Factors Leading to Punchout Development for Improved CRCP Design Procedures," *Proceedings of the 7th International Conference on Concrete Pavements*, pp. 731-745.
33. Parrott, L. J. (July 1988). "Moisture Profiles in Drying Concrete," *Advances in Cement Research,* Vol. 1, No. 3.
34. Van Wijk, A. J. and C. W. Lovell (1986). "Prediction of Subbase Erosion Caused by Pavement Pumping," *Transportation Research Record No. 1099*, Washington, D.C., pp. 45 – 57.
35. Van Wijk, A. J. (1985). "Rigid Pavement Pumping: (1) Subbase erosion and (2) Economic Modeling," Joint Highway Research Project File No. 5-10, School of Civil Engineering, Purdue University, West Lafayette, IN.
36. Bradbury, R. D. (1938). "Reinforced Concrete Pavements," Wire Reinforcement Institute, Washington, D.C.
37. Mohamed, A. R., and W. Hansen (date). "Effect of Nonlinear Temperature Gradient on Curling Stress in Concrete Pavements," *Transportation Research Record No. 1568,* Washington, D.C., pp. 65-71.
38. Poblete, M., P. Ceza, J. David, R. Espinosa, A. Garcia, J. Gonzalez (1991) "A Model of Slab Cracking For PCC Pavements," Transportation Research Record No. 1307, Washington, D.C.
39. Portland Cement Association, Thickness Design for Concrete Pavements, 1966.
40. Smith, K., A. Mueller, M. Darter, and D. Peshkin, "Performance of Jointed Concrete Pavements, Volume II: Evaluation and Modification of Concrete Pavement Design and Analysis Models," Report No. FHWA-RD-89-137, Federal Highway Administration, 1990.
41. Darter, M. and E. Barenberg, "Design of Zero-Maintenance Plain Jointed Pavement, Vol. I – Development of Design Procedures," Report No. FHWA-RD-77-111, April, 1977.
42. Portland Cement Association, Thickness Design for Concrete Pavements, 1984.
43. Poblete, M., R. Salsilli, R. Valenzulea, A. Bull, and P. Spratz, "Field Evaluation of Thermal Deformations in Undoweled PCC Pavement Slabs," Transportation Research Record No. 1207, Transportation Research Board, Washington, D.C., 1988.
44. Poblete, M., A. Garcia, J. David, P. Ceza, and R. Espinosa, "Moisture Effects on the Behavior of PCC Pavements," Proceedings 2nd International Workshop on the Design and the Evaluation of Concrete Pavements, Siquenza, Spain, 1990.
45. Zachlehner, A., "Restraint Stresses in Young Concrete Pavements," Proceedings 6th International Symposium on Concrete Roads, Madrid, Spain, 1990.
46. Janssen, D., "Moisture in Portland Cement Concrete," Transportation Research Record No. 1121, Transportation Research Board, Washington, D.C., 1987.
47. Heath, A. and J. Roesler, "Top-Down Cracking of Rigid Pavements Constructed with Fast-Setting Hydraulic Cement Concrete," Transportation Research Record 1712, Transportation Research Board, Washington, D.C., 20??.
48. Suprenant, B., "Why Slabs Curl, Part I and Par II," Concrete International, American Concrete Institute, March and April, 2002.
49. Armaghani, J., T. Larsen, and L. Smith, "Temperature Response of Concrete Pavements," Transportation Research Record 1121, Transportation Research Board, Washington, D.C., 1987.

50. Eisenmann, J. and G. Leykauf, “Effect of Paving Temperatures on pavement Performance,” Procedings 2nd International Workshop on the Theoretical Design of Concrete Pavements,” Siquenza, Spain, 1990.
51. Eisenmann, J. and G. Leykauf, “Simplified Calculation Method of Slab Curling Caused by Surface Shrinkage,” Proceedings 2nd International Workshop on the Theoretical Design of Concrete Pavements,” Siquenza, Spain, 1990.